A Series of α-Heterocyclic Carboxaldehyde Thiosemicarbazones Inhibit Topoisomerase IIα Catalytic Activity

He Huang,[†,§] Qin Chen,[‡,§] Xin Ku,[†] Linghua Meng,*[,‡] Liping Lin,[‡] Xiang Wang,[‡] Caihua Zhu,[‡] Yi Wang,[‡] Zhi Chen,[†] Ming Li,[‡] Hualiang Jiang,[†] Kaixian Chen,[†] Jian Ding,[‡] and Hong Liu*[,†]

[†]*Drug Discovery and Design Center and* [‡]*Division of Anti-Tumor Pharmacology, State Key Laboratory of Drug Research, Shanghai Institute of Materia Medica, Chinese Academy of Sciences, 555 Zu Chong Zhi Road, Zhangjiang Hi-Tech Park, Shanghai 201203, P. R. China.* [§]*These two authors contributed equally to this work*

Received September 29, 2009

A series of novel thiosemicarbazone derivatives bearing condensed heterocyclic carboxaldehyde moieties were designed and synthesized. Among them, TSC24 exhibited broad antiproliferative activity in a panel of human tumor cells and suppressed tumor growth in mice. The mechanism research revealed that TSC24 was not only an iron chelator but also a topoisomerase IIα catalytic inhibitor. Its inhibition on topoisomerase IIα was due to direct interaction with the ATPase domain of topoisomerase IIα which led to the block of ATP hydrolysis. Molecular docking predicted that TSC24 might bind at the ATP binding site, which was confirmed by the competitive inhibition assay. These results about the mechanisms involved in the anticancer activities of thiosemicarbazones will aid in the rational design of novel topoisomerase II-targeted drugs and will provide insights into the discovery and development of novel cancer therapeutics based on the dual activity to chelate iron and to inhibit the catalytic activity of topoisomerase IIα.

1. Introduction

The thiosemicarbazone (TSC) is considered as one of the most important scaffolds and is embedded in many biologically active compounds.[1−8] Brockman et al. first showed that 2-formylpyridine TSC possesses antileukemic activity in mice bearing leukemic cells.[9] Following this report, various aliphatic, aromatic, and heteroaromatic carbaldehyde TSCs were synthesized and evaluated for antitumor activity against a wide spectrum of transplanted murine neoplasms.[1,10−16] Examples of TSC derivatives demonstrating profound anticancer activities are presented in Figure 1. To date, the most significant progress in the treatment of cancer has been made with 3-aminopyridine-2-carboxaldehyde TSC (3-AP or triapine) which is currently in phase II clinical trials. Generally, the TSCs derived from five- or six-member heterocycle scaffolds possess potent anticancer activity, which is exemplified by 2-pyridine carbaldehyde derivatives, including 3-AP. However, the therapeutic potential of 3-AP was limited by its poor water solubility and toxicity profile.[17] Therefore, there is increasing interest in structural modification of TSC derivatives with the aim of improving the pharmaceutical profile of existing candidates or of discovering novel derivatives. Up to now, most of the structure−activity relationship studies reported were focused on substitutions at the heterocycle core structure. Few data have been published describing the antitumor activity of heteroaromatic compounds that contain a condensed heterocycle.

TSCs were considered to suppress tumor growth by virtue of their ability to chelate iron (Fe).[18−22] They are capable of removing Fe from biological systems and inhibit the activity of Fe-requiring proteins, including ribonucleotide reductase (RR[a]), a key enzyme involved in DNA synthesis and repair. Because neoplastic cells have a higher requirement for iron than healthy cells because of their rapid proliferation, TSCs selectively inhibit the proliferation of tumor cells. Meanwhile, several studies provided evidence indicating that TSCs exert their antitumor functions via more than Fe chelating. First, complexation to metal can potentiate rather than weaken the antitumor activities of some TSCs.[23,24] Second, Fe chelation induces an arrest of the cell cycle at the S phase due to the inhibition of DNA synthesis. In contrast, an accumulation of cells at the G2/M phase or no change in cell cycle is often noticed after TSC treatment.[1,11] Therefore, the mechanisms involved in the antitumor activities of TSCs are far from clear.

In an effort to discover novel TSC derivatives with potent anticancer activity and to elucidate their mechanism of action, TSCs bearing condensed heterocyclic carboxaldehyde moieties were synthesized and their antitumor activities were evaluated. We found that several compounds exhibited potent cytotoxic activity in tumor cells. Among them, TSC24, which is the most active in the primary screening, displayed broad antiproliferative activity in a panel of human tumor cells including multidrug resistant cells. TSC24 displayed profound

*To whom correspondence should be addressed. For L.M.: phone, +86-21-50806722; fax, +86-21-50806722; e-mail, lhmeng@mail.shcnc.ac.cn. For H.L.: phone, +86-21-50807042; fax, +86-21-50807088; e-mail, hliu@mail.shcnc.ac.cn.

[a] Abbreviations: RR, ribonucleotide reductase; DSBs, double strand breaks; At-MDR, altered topoisomerase II-associated multidrug resistance; Topo, topoisomerase; VP16, etoposide; Acl, aclarubicin; ADR, adriamycin; CPT, camptothecin; EB, ethidium bromide; m-AMSA, amsacrine; HsATPase, human topoisomerase IIα ATPase domain; SPR, surface plasmon resonance spectroscopy.
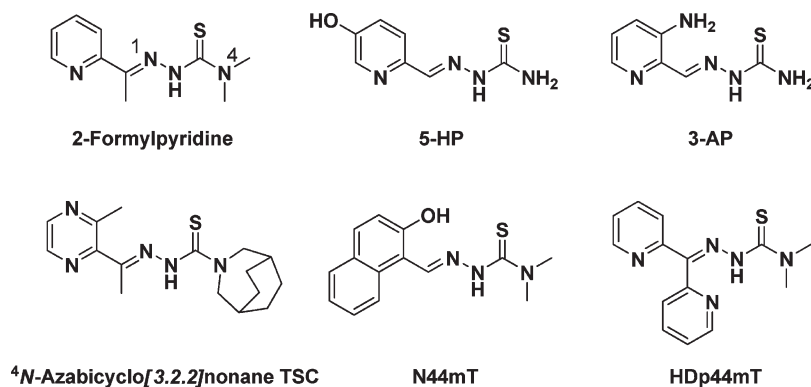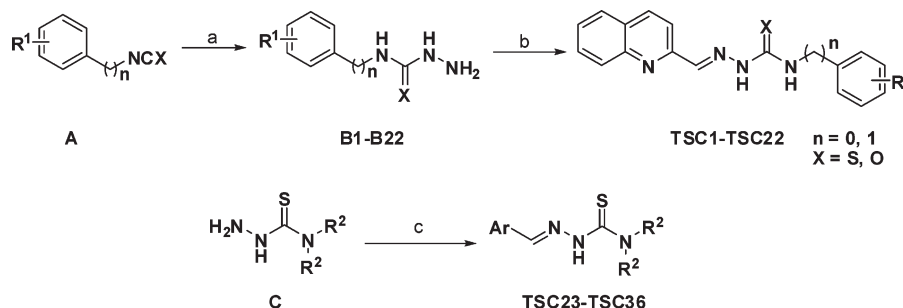
Figure 1. Structures of some TSC derivatives demonstrating profound anticancer activities.

Scheme 1. Procedure for the Synthesis of α-Heterocyclic Carboxaldehyde Thiosemicarbazones[a]

[a] Reagents and conditions: (a) hydrazine hydrate (85%), isopropanol, room temp; (b) quinoline-2-carbaldehyde, isopropanol, acetic acid (cat.), room temp; (c) α-heterocyclic carboxaldehyde, isopropanol, microwave irradiation, 100 °C, 30 min.

activity in mice bearing S-180 sarcoma. Importantly, the mechanistic studies revealed that TSC24 is a new topoisomerase IIα (Topo IIα) catalytic inhibitor in addition to its Fe chelating ability. By dissecting the effect of TSC24 on the individual steps of the catalytic cycle of Topo IIα, we found that TSC24 blocked Topo IIα-catalyzed ATP hydrolysis by competing with ATP for binding to the ATPase domain of Topo IIα.

2. Materials and Methods

2.1. Chemical Design and Synthesis. On the basis of the structural features of reported compounds, 36 new analogues (TSC1–TSC36) were designed and synthesized. Keeping the quinoline ring at N^1 position, we obtained compounds TSC1–TSC24 by introducing diverse groups to the N^4 position. And by replacing the quinoline rings of TSC23 and TSC24 with the diverse condensed heteroaromatic rings, we got compounds TSC25–TSC36. Synthesis of these TSC derivatives was straightforward following the general procedures outlined in Scheme 1. The N^4 substituted TSC derivatives **B** were prepared through the nucleophilic addition reaction of 85% hydrazine hydrate with various iso(thio)cyanates **A** at room temperature. Compounds **B1–B22** were condensed with quinoline-2-carbaldehyde in isopropanol for 2 h, affording TSC1–TSC22, respectively. Commercially available compounds **C** were successfully converted to target compounds TSC23–TSC36 by condensation of respective hydrazines to the appropriate aldehydes under microwave irradiation in isopropanol for 30 min.

2.2. In Vitro Cytotoxicity Assays. The cytotoxic activities of the compounds were evaluated using human acute leukemia HL-60, human gastric cancer SGC7901, human cervical cancer HeLa, and human colon carcinoma HT-29 cells. Cells seeded in 96-well plates were treated in triplicate with gradient concentrations of compounds for 72 h. For suspended cells, cytotoxicity was assessed by measuring the conversion of 3-(4,5-dimethylthiazol-2-yl)-2,5-diphenyltetrazolium bromide (Sigma, St. Louis, MO) to a colored product.[25] Sulforhodamine B assay (Sigma, St. Louis, MO) was applied to detect the cytotoxicity in adherent cells.[26] The concentration required for 50% inhibition of cell growth compared with control cells (IC_{50}) was determined by the Logit method. TSC24 was further evaluated for its antiproliferative activity against a panel of human tumor cells originated from different tissue types, including colon cancer, gastric cancer, breast cancer, lung cancer, hepatocellular cancer, leukemia, melanoma, rhabdomyosarcoma, cervical cancer, and oral squamous carcinoma.

2.3. In Vivo Antitumor Studies. In vivo antitumor studies were carried out with compound TSC24 in 7-week-old female Kunming mice (weight, 18–22 g) provided by the Shanghai Laboratory Animal Center, Chinese Academy of Sciences. Mice were inoculated sc into the right armpit with S-180 sarcoma. On the next day, normal saline or 5-fluorouracil was administered by iv injection, and TSC24 was administered at indicated doses by ip injection for 7 days. After treatment, animals were killed by cervical dissociation, and solid tumors were removed and weighed. The inhibitory rate was calculated as the following formula: inhibitory rate (%) = {[(mean tumor weight of control group) − (mean tumor weight of treatment group)]/(mean tumor weight of control group)} × 100%.

2.4. Fenton's Reaction-Mediated Plasmid DNA Breaks. The effect of compounds on the integrity of plasmid DNA was analyzed as described previously.[27] Briefly, pBR322 plasmid (0.2 μg) was incubated with reaction buffer containing 13 mM 4-(2-hydroxyethyl)-1-piperazineethanesulfonic acid (Hepes, pH 7.2), 1 mM H_2O_2, and 10 μM $FeSO_4$ in the presence of indicated concentrations of desferrioxamine (DFO) or TSC24. After incubation at room temperature for 30 min, samples were immediately loaded with 5 μL of loading dye onto a 1% agarose gel containing 0.1 μg/mL ethidium bromide (EB). The gels were run at 90 V for 60 min, then visualized using a UV transilluminator and photographed. The intensity of DNA bands was quantified and the percentage of supercoiled plasmid DNA was calculated with the formula % SC = [1.4 SC/(L + OC + 1.4 SC)] × 100.

A correction factor of 1.4 was applied to count the relatively attenuated fluorescence of supercoiled (SC) DNA compared to the open-circular (OC) and linear (L) forms.[27]

2.5. Flow Cytometric Analysis of BrdU Incorporation and Cell Cycle Distribution. DNA synthesis was measured by BrdU incorporation assay using BrdU flow kit (BD Pharmingen, San Diego, CA) according to the manufacturer's instructions. Cell cycle analyses were performed on a FACS Calibur cytometer (Becton Dickinson, Mountain View, CA) after cells were stained with propidium iodide (PI). Cell cycle distributions were analyzed using ModFit LT 3.0 software (Verity Software House Inc., Topsham, ME).

2.6. Topo I- and Topo IIα-Mediated Supercoiled pBR322 Relaxation Assay and Topo IIα-Mediated kDNA Decatenation Assay. Relaxation and decatenation assays were carried out as previously described.[28] Briefly, reaction buffer contained 50 mM Tris-HCl (pH 8.0), 120 mM KCl, 10 mM MgCl$_2$, 0.5 mM DTT, 1 mM ATP (ATP was omitted in Topo I-mediated DNA relaxation), 0.25 μg of supercoiled pBR322 or 0.1 μg kDNA, 1 unit of Topo I or Topo IIα in a total volume of 20 μL. After incubation at 37 °C for 15 min, the reaction was terminated by the addition of 1 μL of SDS (10%). The DNA samples were mixed with loading buffer and subjected to electrophoresis in 1% agarose gel in TAE buffer at 90 V for 60 min.

2.7. Topo II-Mediated DNA Cleavage Assay. Prestrand passage DNA cleavage reactions were carried out in a final volume of 20 μL, containing 50 mM Tris-HCl (pH 8.0), 120 mM KCl, 10 mM MgCl$_2$, 0.5 mM DTT, 0.25 μg of supercoiled pBR322, and 10 units of Topo IIα. In the complete cleavage reactions, 1 mM ATP was included. After incubation at 37 °C for 15 min and the reaction stopped by the addition of 1 μL of SDS (10%), the reaction mixtures were incubated with 2 μL of proteinase K (0.8 mg/mL) at 45 °C for 30 min to digest the Topo IIα. Final products were mixed with loading buffer, heated at 70 °C for 2 min, and subjected to electrophoresis in 1% agarose.

2.8. Neutral Single-Cell Gel Electrophoresis Assay. HT-29 cells were pretreated with TSC24 or aclarubicin for 30 min, then exposed to 10 μM VP16 for 1 h. DNA double-strand breaks (DSBs) were evaluated by neutral single-cell gel electrophoresis assay as described.[29,30] The images were captured with a fluorescence microscope (Olympus BX51, Olympus Co., Tokyo, Japan).

2.9. TSC24−DNA Interaction. A topoisomerase I unwinding assay and an ethidium bromide (EB) displacement fluorescence experiment were performed to examine the ability of TSC24 to intercalate into plasmid DNA as described.[31,32] To determine whether TSC24 binds to the minor groove of DNA, a Hoechst 33258 displacement experiment was performed.[32]

2.10. Topo II−DNA Binding Assay. Topo II−DNA binding was evaluated by an electrophoretic mobility shift assay.[33] Reactions were carried out in 20 μL of reaction buffer containing 0.2 μg of supercoiled pBR322 DNA and 200 nM human topo IIα in the presence or absence of TSC24. After incubation at 37 °C for 10 min, samples were separated on a 1% agarose gel containing 0.5 μg/mL EB by electrophoresis for 90 min in TAE buffer.

2.11. Purification of the Human Topoisomerase IIα ATPase Domain (HsATPase) and ATP Hydrolysis Assay. HsATPase was expressed and purified as described previously.[34,35] The ATP hydrolysis catalyzed by HsATPase was coupled to the oxidation of NADH.[17] The reactions were carried out in 96-well plates at 37 °C in a total volume of 100 μL containing 2 μg of HsATPase or 18 nM Topo IIα, 0.2 μg of pBR322 DNA, 1 mM ATP, 2 mM PEP, 0.16 mM NADH, 5 U of pyruvate kinase, and 8 U of lactate dehydrogenase. The OD values of NADH were monitored by a spectrophotometer (VERSAmax; Molecular Devices, Sunnyvale, CA), which was programmed to collect data every 20 s at 340 nm.

2.12. Surface Plasmon Resonance Spectroscopy (SPR). The SPR assay was performed at 25 °C using a Biacore 3000 instrument (Biacore AB, Uppsala, Sweden). HsATPase was immobilized onto CM5 sensor chips after activation of the surface carboxyl groups as previously reported.[35] Serial dilutions of compounds were injected to flow across the chip surface, and sensorgrams were recorded. Equilibrium constants (K_D) for evaluating protein−ligand binding affinity were determined using the steady-state affinity fitting analysis.

2.13. Molecular Docking. The crystal structure of HsATPase in complex with ADPNP was retrieved from the Protein Data Bank (PDB entry 1ZXM). DOCK 4.0 was used to predict the potential binding between TSC24 and HsATPase. For the target, the Connolly molecular surface was calculated with a probe radius of 1.4 Å. The residues around the cocrystallized ligand within 7 Å were defined as binding site with Sybyl 6.8 (Tripos Associates Inc., St. Louis, MO). Within the binding site, spheres were generated therein with the DOCK program SPHGEN. SPHGEN outputted the spheres in clusters. The spheres within 5 Å radius of the natural ligand were selected for the target. The compound was docked into the binding site, allowing for ligand flexibility, using the grid-based energy scoring option for minimization after initial placement in the site. The box for the scoring grid was defined such that all spheres were enclosed with an extra 7 Å added in each dimension. Scoring grids for contact and energy scores were calculated with a grid spacing of 0.3 Å. The bump check was set such that atoms closer than 75% of the van der Waals radii of the respective atoms were rejected. A 6−12 Lennard-Jones van der Waals potential was used along with a Coulomb potential using a distance-dependent dielectric coefficient of 4 to simulate salvation effects. The energy cutoff was set to 10 Å. The radii used were those in the vdw.defn set. Ligand atoms were matched to receptor spheres using the anchor first search with the anchor size set to 10 atoms. The automatic matching option was used, and conformations were generated with the torsion drive option.

2.14. Statistical Analysis. All data were expressed as mean values ± SD. At least three independent experiments were conducted in triplicate. Statistical analysis was performed by unpaired Student's *t* test. A *p* value less than 0.05 was considered to be statistically significant.

3. Results

3.1. Chemistry. The chemical structures of the 36 newly synthesized compounds (TSC1−TSC36) are shown in Table 1. These compounds were synthesized through the routes outlined in Scheme 1, and the details of the synthetic procedures and structural characterizations are described in the Experimental Section.

3.2. In Vitro Antitumor Studies. 3.2.1. Effects of TSCs on the Proliferation of Tumor Cells. All substances were evaluated for antiproliferative activites against the human acute leukemia (HL-60) cell line, human gastric cancer (SGC7901) cell line, human cervical cancer (Hela) cell line, and human colon carcinoma (HT-29) cell line. The data shown in Table 1 are IC$_{50}$ values against tested tumor cells. The compounds bearing alkyl groups at the N^4 position showed promising antiproliferative activity, while the unsubstituted and aryl-substituted derivatives at this position displayed low or moderate activity. Of all the compounds tested, TSC24 showed the best antitumor efficacy, with an IC$_{50}$ ranging from 0.02 to 0.09 μM without distinct selectivity among the cell lines tested. TSC26, TSC28, TSC31, and TSC36 (average IC$_{50}$ values on four cell lines are 0.36, 0.64, 1.71, and 0.56 μM, respectively) also demonstrated appreciable antiproliferative activities.

3.2.2. TSC24 Exhibits Broad Antiproliferative Activity against Tumor Cells. TSC24 showed potent antiproliferative activity with IC$_{50}$ values in the nanomolar range against a panel of human tumor cells, including colon cancer, gastric cancer, breast cancer, lung cancer, hepatocellular cancer,

Table 1. Inhibition of Cell Proliferation of Thiosemicarbazones
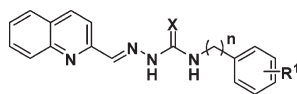
Compound	n	X	R^1	IC$_{50}$ (mean ± SD), μM			
				HL-60	SGC-7901	Hela	HT-29
TSC1	0	S	-H	9.13 ± 1.80	26.48 ± 8.36	27.39 ± 4.95	16.99 ± 3.69
TSC2	0	S	2-OMe	91.69 ± 11.03	>100	>100	>100
TSC3	0	S	3-OMe	71.22 ± 15.60	79.41 ± 6.61	74.50 ± 3.31	82.35 ± 19.24
TSC4	0	S	4-OMe	43.78 ± 6.09	89.57 ± 10.71	72.63 ± 5.02	82.29 ± 16.83
TSC5	0	S	2-Me	73.20 ± 14.57	>100	>100	42.25 ± 10.88
TSC6	0	S	3-Me	>100	>100	>100	>100
TSC7	0	S	4-Me	78.32 ± 12.56	92.90 ± 8.64	86.00 ± 4.34	85.53 ± 15.68
TSC8	0	O	4-Me	>100	>100	>100	>100
TSC9	0	S	2-F	>100	>100	>100	>100
TSC10	0	S	3-F	43.78 ± 9.97	79.87 ± 5.28	70.13 ± 0.56	74.71 ± 13.06
TSC11	0	S	4-F	16.98 ± 4.26	32.27 ± 9.33	33.17 ± 10.19	28.50 ± 8.68
TSC12	0	S	3-Cl	28.80 ± 26.27	61.29 ± 5.70	52.50 ± 5.67	48.10 ± 12.05
TSC13	0	S	4-Cl	>100	87.60 ± 1.51	>100	97.18 ± 20.90
TSC14	0	S	2-Br	>100	>100	>100	>100
TSC15	0	S	3-Br	53.83 ± 31.64	78.59 ± 1.91	69.98 ± 1.95	58.94 ± 12.73
TSC16	0	S	4-Br	27.46 ± 25.83	69.39 ± 6.44	56.81 ± 14.37	54.35 ± 13.31
TSC17	0	S	2-CF$_3$	13.17 ± 6.17	20.69 ± 2.71	18.80 ± 4.93	18.11 ± 3.57
TSC18	0	S	4-CF$_3$	34.87 ± 20.49	72.19 ± 6.11	59.13 ± 3.31	63.88 ± 2.29
TSC19	0	S	4-CN	4.66 ± 0.46	23.69 ± 4.88	20.04 ± 1.95	15.55 ± 2.36
TSC20	0	S	2,6-diisopropylphenyl	19.47 ± 2.47	23.48 ± 2.63	16.35 ± 2.68	20.68 ± 2.75
TSC21	0	S	2-OMe-5-Me	>100	>100	>100	>100
TSC22	1	S	-H	21.90 ± 0.33	53.68 ± 16.34	62.81 ± 5.78	75.65 ± 22.46
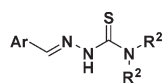
Compound	R^2	Ar	IC$_{50}$ (mean ± SD), μM			
			HL-60	SGC-7901	Hela	HT-29
TSC23	-H		>100	32.70 ± 9.94	0.96 ± 0.45	>100
TSC24	-CH$_3$		0.05 ± 0.01	0.03 ± 0.00	0.09 ± 0.02	0.02 ± 0.01
TSC25	-H		>100	>100	>100	>100
TSC26	-CH$_3$		0.09 ± 0.01	0.17 ± 0.04	0.75 ± 0.12	0.45 ± 0.25
TSC27	H		>100	>100	>100	12.83 ± 2.74

Table 1. Continued
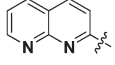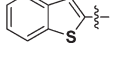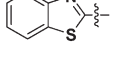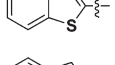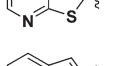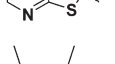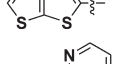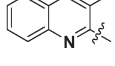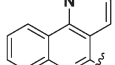
Compound	R^2	Ar	IC$_{50}$ (mean ± SD), μM			
			HL-60	SGC-7901	Hela	HT-29
TSC28	-CH$_3$		0.56 ± 0.00	0.63 ± 0.13	0.97 ± 0.04	0.41 ± 0.14
TSC29	-H		>100	>100	6.77 ± 2.34	99.16 ± 24.15
TSC30	-H		>100	>100	5.35 ± 1.23	>100
TSC31	-CH$_3$		3.68 ± 0.97	0.83 ± 0.07	2.10 ± 0.00	0.25 ± 0.09
TSC32	-H		>100	>100	6.29 ± 3.68	>100
TSC33	-CH$_3$		>100	21.417 ± 1.238	48.41 ± 24.34	13.38 ± 4.08
TSC34	-H		>100	>100	1.12 ± 0.18	57.50 ± 14.54
TSC35	-H		>100	7.36 ± 3.33	21.92 ± 1.26	11.52 ± 3.83
TSC36	-CH$_3$		0.43 ± 0.11	0.04 ± 0.00	1.72 ± 0.07	0.04 ± 0.05

Table 2. Inhibition of Cell Proliferation of Compounds TSC24 against a Panel of Human Tumor Cells

	cell line					
	colon			stomach		
	HT29	HCT116	Lovo	MKN45	MKN28	SGC-7901
IC$_{50}$ (mean ± SD), μM	0.02 ± 0.01	0.22 ± 0.10	0.06 ± 0.03	0.83 ± 0.14	0.17 ± 0.02	0.03 ± 0.00

	cell line				
	breast			lung	
	MDA-MB-231	MCF-7	MDA-MB-435	NCI-H23	A549
IC$_{50}$ (mean ± SD), μM	0.02 ± 0.02	0.34 ± 0.19	0.37 ± 0.17	0.08 ± 0.06	0.45 ± 0.35

	cell line				
	liver			blood	
	BEL-7402	SMMC-7721	HL-60	K562	U-937
IC$_{50}$ (mean ± SD), μM	0.18 ± 0.12	0.24 ± 0.01	0.05 ± 0.01	0.06 ± 0.05	0.03 ± 0.01

	cell line other			
	A375	Rh30	Hela	KB
IC$_{50}$ (mean ± SD), μM	0.02 ± 0.01	0.002 ± 0.000	0.09 ± 0.02	0.77 ± 0.19

leukemia, melanoma, rhabdomyosarcoma, cervical cancer, and oral squamous carcinoma (Table 2). Meanwhile, TSC24 did not show obvious selectivity against these tumor cells.

3.2.3. TSC24 Overcomes Multidrug Resistance. MDR is considered to be an important impediment to the effective chemotherapy of cancer. We next investigated the cytotoxicity of TSC24 in three MDR cell lines: K562/A02, MCF-7/ADR, and KB/VCR. Resistance factor (RF), defined as the ratio of the IC$_{50}$ against resistant cells to that against the corresponding parental cells (K562, MCF-7 or KB), was

Table 3. Resistance Factors of TSC24 and Reference Drug in MDR Sublines[a]

compd	IC$_{50}$ (mean ± SD), μM					
	K562	K562/A02	KB	KB/VCR	MCF-7	MCF-7/ADR
TSC24	0.16 ± 0.04	0.06 ± 0.03	0.78 ± 0.19	0.30 ± 0.09	0.34 ± 0.19	0.20 ± 0.02
ADR	0.43 ± 0.17	23.81 ± 2.99	NT[b]	NT[b]	0.39 ± 0.12	44.9 ± 1.27
VCR	NT[b]	NT[b]	0.01 ± 0.00	0.84 ± 0.08	NT[b]	NT[b]

compd	resistance factor		
	K562/A02	KB/VCR	MCF-7/ADR
TSC24	0.37	0.39	0.57
ADR	55.93	NT[b]	115.13
VCR	NT[b]	119.71	NT[b]

[a] Cells were treated with indicated compounds for 72 h, and IC$_{50}$ values were determined by using 3-(4,5-dimethylthiazol-2-yl)-2,5-diphenyl-tetrazolium bromide or sulforhodamin B assays. [b] NT: not tested.

Table 4. TSC24 Inhibited Tumor Growth in Mice Implanted with S-180 Sarcoma Cells[a]

treatment group	dosage ((mg/kg)/day) × day	mice number		body weight (g)		tumor weight, x ± SD (g)	inhibition rate (%)	P
		initial	end	initial	end			
NS		20	20	18.1	32.5	1.76 ± 0.36		
TSC24	50 × 7 (ip)	10	10	17.9	20.0	0.44 ± 0.33	76.7	< 0.01
TSC24	25 × 7 (ip)	10	10	17.9	23.9	1.13 ± 0.55	35.8	
TSC24	12.5 × 7 (ip)	10	10	17.9	29.0	1.45 ± 0.55	17.6	
5-Fu	50 × 2 (iv)	10	10	18.1	27.5	0.34 ± 0.22	80.7	< 0.01

[a] Mice received S-180 cells were given a daily ip administration of saline (NS) or TSC24 for the next 7 days or following an iv administration of 5-Fu twice a week, at the doses shown. Inhibition rate (%) = {[(mean tumor weight of NS treatment) − (mean tumor weight of TSC24 or 5-Fu treatment)]/(mean tumor weight of NS treatment)} ×100%. *P*-values were derived using a one-tailed *t* test.

calculated. The RF values for doxorubicin (ADR) in K562/A02 and MCF-7/ADR cell lines and for vincristine (VCR) in KB/VCR cell line were 55.93, 115.12, and 119.71, respectively, which confirmed that the cells utilized remained their MDR phenotype. In contrast, TSC24 was more potent against MDR sublines compared to the parental cells, with RF values of 0.37−0.57 (Table 3). These results demonstrate that TSC24 significantly overcomes multidrug resistance.

3.3. In Vivo Antitumor Studies. The anticancer activity of TSC24 in vivo was evaluated in S-180 sarcoma-bearing mice. As shown in Table 4, TSC24 inhibited tumor growth in a dose-dependent manner, with inhibitory rates of 17.6%, 35.8%, and 76.7% at doses of 12.5, 25, and 50 (mg/kg)/day, respectively, after it was administered ip for 7 days.

3.4. Iron Chelation of Compound TSC24. 3.4.1. TSC24 Chelates Fe and Arrests the Cell Cycle at the G1/S Boundary. The reaction between Fe(II) and hydrogen peroxide, namely, Fenton's reaction, results in the generation of highly reactive hydroxyl radicals, which could cause damage to various biomolecules, such as DNA. A single-strand break in DNA causes the conversion of supercoiled (SC) DNA to the open-circular (OC) form, while a double-strand break results in the conversion of SC DNA to the linear (L) form. As shown in Figure 2A, control supercoiled plasmid and hydrogen peroxide-treated plasmid appeared on gels predominately as a single SC DNA band. When plasmid was incubated with Fe(II) and hydrogen peroxide, SC DNA partially converted to the L and OC forms. TSC24 treatment prevented Fenton's reaction-mediated strand breaks in plasmid DNA, indicating that chelation of Fe by TSC24 abrogated Fenton's reaction-mediated DNA breaks. A similar result was obtained in the presence of DFO, which is a well-known Fe chelator. Quantitation of the intensity of DNA breaks was plotted and depicted in Figure 2A. Both TSC24 and DFO prevented DNA breaks in concentration-dependent manners. However, TSC24 possessed much higher affinity for Fe(II) than DFO because inhibition of DNA breaks in

the presence of 1 μM TSC24 was very close to that in the presence of 100 μM DFO.

Inactivation of RR by Fe chelation in cells results in inhibition of DNA synthesis. A BrdU incorporation assay was performed to measure DNA synthesis. As shown in Figure 2B, DNA synthesis was inhibited by TSC24 in concentration- and time-dependent manners. Agents capable of inhibiting DNA synthesis might result in G1/S or S cell cycle arrest. To investigate the effect of TSC24 on cell cycle progression, HT-29 cells were exposed to TSC24 for 24 h. As shown in Figure 2C (−Aph), TSC24 induced G1 arrest in exponentially growing cells. To distinguish the G1 phase from the G1/S boundary, HT-29 cells were synchronized at the G1/S boundary by treatment with the DNA polymerase inhibitor aphidicolin. One hour after removal of aphidicolin, synchronized cells were treated with nocodazole in the presence or absence of TSC24 for 24 h. The cell cycle progressed and was arrested in the M phase by Nocdazole, while the cell cycle failed to move forward after being released from the G1/S boundary in the presence of TSC24 and nocodazole (Figure 2C, +Aph), indicating that TSC24 arrested cells at the G1/S boundary. This finding was in line with its ability to inhibit DNA synthesis. Considering that the dose range of TSC24 to inhibit Fenton's reaction-mediated DNA strand breaks is similar to that to inhibit BrdU incorporation assay, we propose that TSC24 might chelate iron and inactivate RR in cells. However, we cannot rule out the involvement of other mechanisms in the TSC24-induced DNA synthesis inhibition and cell cycle arrest.

3.4.2. Supplementation of Fe Partially Reverses the Cytotoxicity of TSC24. To determine whether the antiproliferative activity of TSC24 was dependent on Fe chelation, HT-29 cells were treated with TSC24 alone or in the presence of Fe. FeSO$_4$ (50 μM) had no effect on cell growth in the absence of drug (data not shown). As shown in Figure 2D, supplementation of Fe impaired the cytotoxicity of TSC24 in HT-29
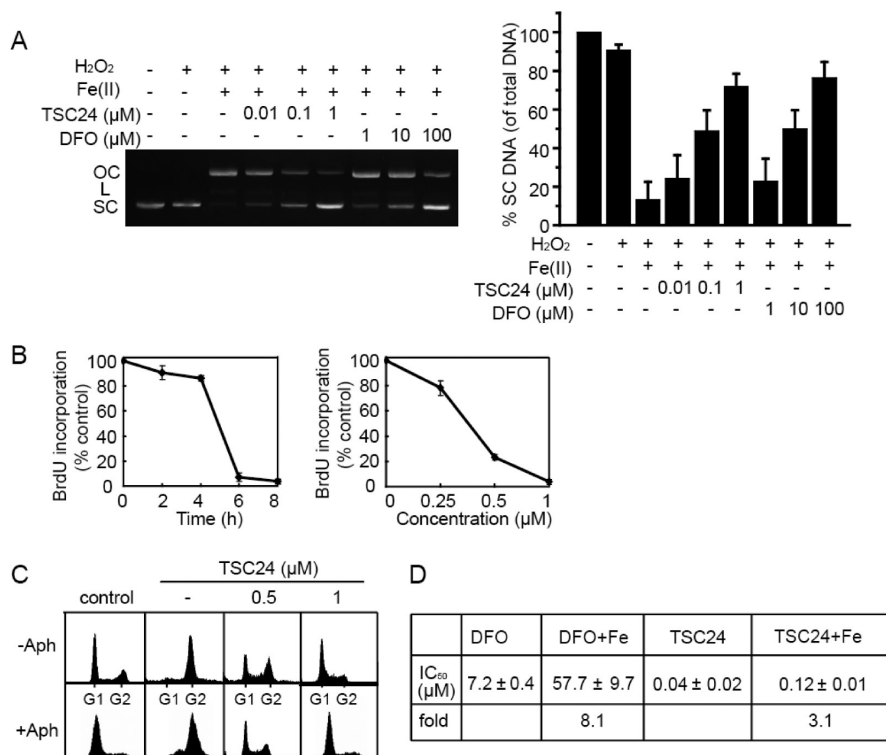
Figure 2. TSC24 is a Fe chelator. (A) TSC24 prevented Fenton's reaction-mediated strand breaks in plasmid DNA. Image shown is representative of three experiments, and data plotted are the mean ± SD of three separate experiments. (B) TSC24 inhibited DNA synthesis. After treatment with TSC24 for the indicated time, HT29 cells were labeled with BrdU and incubated with anti-BrdU antibody: (left) time course with 1 μM TSC24; (right) concentration response with TSC24 for 8 h. (C) TSC24 arrested cell cycle at G1/S boundary: (top) asynchronous cells were exposed to nocodazole (0.5 μg/mL) alone or in association with TSC24 for 24 h; (bottom) after synchronized with aphidicolin (Aph, 4 μg/mL) for 24 h and released for 1 h, cells were further treated with nocodazole in the presence or absence of TSC24 for 24 h. DNA content distribution was measured by flow cytometry. (D) Supplement of Fe partially reversed the cytotoxicity of TSC24 against HT-29 cells. Cells seeded in 96-well plates were treated with the indicated compounds in the presence or absence of FeSO$_4$ (50 μM) for 72 h. IC$_{50}$ values are shown as the mean ± SD of three separate experiments.

cells, demonstrated as a much higher IC$_{50}$, further supporting the notion that TSC24 could chelate iron in cells, which contributed to the antiproliferative activity of TSC24. However, the IC$_{50}$ of TSC24 increased about 3-fold upon Fe supplementation, which was much lower than that of DFO (about 8-fold), suggesting that other mechanism(s), which could not be abrogated by Fe supplementation, might also be involved in the antitumor activity of TSC24.

3.5. TSC24 Inhibits Topo IIα Catalytic Activity. 3.5.1. TSC24 Inhibits the Catalytic Activities of Human Topo IIα and Arrests Synchronized Cells at the M Phase. To predict the potential mechanisms of TSC24, the COMPARE program (http://dtp.nci.nih.gov/) was run to compare the antiproliferative profiles of TSC in NCI 60 human cancer cell lines (NCI-60) to those of designated standard agents. TSC derivatives were found to highly positively correlate with Topo II inhibitors in their anticancer profiles against NCI-60. Sporadic reports have also revealed that TSC derivatives were likely to target Topo II.[16,36] To explore whether TSC24 could also inhibit Topo II, the effect of TSC24 on the catalytic activity of human Topo IIα was evaluated using human Topo IIα-mediated pBR322 relaxation and kDNA decatenation assays. As shown in Figure 3A, TSC24 significantly inhibited the relaxation of supercoiled pBR322 in a concentration-dependent manner. Most of pBR322 plasmids remained in a supercoiled form in the presence of 25 μM TSC24. Similarly, almost all the catenated DNA substrate (kDNA) remained in the wells after treatment with 25 μM TSC24 (Figure 3B), indicating the inhibition of Topo IIα

catalytic activity by TSC24. However, the inhibition of Topo IIα by TSC24 was independent of its Fe chelating ability because other Fe chelators such as DFO and 3-AP could not inhibit Topo IIα-mediated pBR322 relaxation (Figure 3A).

The Topo I-mediated supercoiled pBR322 relaxation assay was carried out subsequently to test the effect of TSC24 on the catalytic activity of Topo I. Results presented in Figure 3C show that camptothecin (CPT) strongly inhibited Topo I-mediated supercoiled pBR322 relaxation, while TSC24 had no inhibitory effect on Topo I even at the highest concentration examined.

Topo IIα has essential roles in sister chromatid separation at anaphase,[37] so Topo II inhibitors could arrest the cell cycle at the M phase. In order to exclude the effect of Fe chelation, cells were synchronized at the M phase by treatment with nocodazole for 24 h and then released from the M phase by washing out the nocodazole. After further incubation in fresh medium for 1 h, cells were treated with TSC24 for 24 h (Figure 3D). Cells went through mitosis after the nocodazole was removed (Figure 3D, T24). Similar results were obtained in the presence of DFO and 3-AP (Figure 3D, DFO and 3-AP), which was in agreement with their failure to inhibit the catalytic activity of Topo II. In contrast, cells were allowed to accumulate at the M phase in the presence of TSC24 (Figure 3D, TSC24), which was consistent with the fact that TSC24 inhibited the catalytic activity of Topo II.

To test whether the inhibitory action of Top II is universal to TSCs and related to their antitumor activity, the effects of
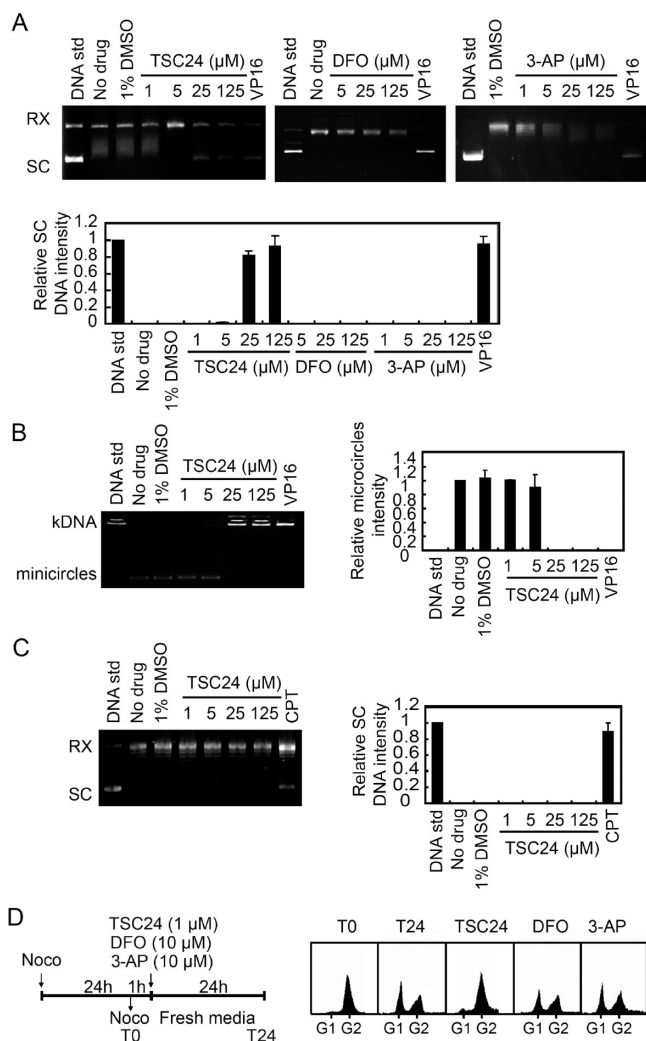
Figure 3. TSC24 inhibits the catalytic activity of topo IIα. (A) TSC24 inhibited Topo IIα-mediated supercoiled DNA relaxation. Plasmid pBR322 was incubated with Topo IIα alone or in association with the indicated compounds at 37 °C for 30 min. VP16 (100 μM) was employed as a positive control. The positions of supercoiled DNA (SC) and relaxed DNA (RX) are indicated. (B) Effect of TSC24 on Topo IIα-catalyzed kDNA decatenation. (C) TSC24 was unable to inhibit Topo I-mediated supercoiled DNA relaxation. Camptothecin (CPT, 100 μM) was included as a positive control. The images of (A), (B), and (C) are densitometric analyzed, and data plotted are the mean ± SD of three separate experiments. (D) TSC24 arrested synchronized cells at the M phase. After synchronization by nocodazole (Noc, T0), HT-29 cells were further incubated in fresh medium in the absence (T24) or presence of TSC24 (1 μM), DFO (10 μM), and 3-AP (5 μM) for 24 h.

all the compounds on the catalytic activity of human Topo II were evaluated using the human Topo II-mediated kDNA decatenation assay. As shown in Figure 4, seven compounds (TSC24, TSC26, TSC28, TSC31, TSC33, TSC35, and TSC36) completely inhibited the catalytic activity of Topo II at 100 μM, while another seven compounds (TSC5, TSC10, TSC23, TSC27, TSC29, TSC30, and TSC34) displayed moderate inhibitory activity and the rest of the compounds had little activity in this reaction. It is noteworthy that inhibitory activities of tested compounds against Topo II positively correlated with their antiproliferative activities in tumor cells; i.e., compounds such as TSC24 displaying superior activity against Topo II are more potent to inhibit tumor cell proliferation.

3.5.2. TSC24 Acts as a Catalytic Inhibitor of Human Topo IIα. HL-60/MX2 is a cell line derived from HL-60 cells selected for resistance to mitoxantrone, which displays atypical multidrug resistance (at-MDR) with altered Topo II catalytic activity and reduced levels of Topo IIα and Topo IIβ proteins.[38] For HL-60/MX2 cells, a decrease in Topo II activity led to a reduced level of DNA damage and therefore resistance to Topo II poison. Cell killing by Topo II catalytic inhibitor depends on the inhibition of Topo II, so the pattern of sensitivity of such agents is opposite to that for Topo II poisons. Cells with reduced Topo II activity are sensitive to Topo II catalytic inhibitor.[39] As shown in Figure 5A, HL-60/MX2 cells were resistant to the Topo II poison etoposide (VP16), while they exhibited little cross-resistance to the catalytic inhibitor aclarubicin (Acl). We found that HL-60/MX2 cells were sensitive to TSC24, with an IC$_{50}$ lower than that of parental HL-60 cells (Figure 5A). On the basis of the fact that TSC24 inhibited activity of Topo II in cell-free system and exhibited the same cytotoxicity pattern against HL-60/MX2 cells as aclarubicin, we proposed that TSC24 might act as a Topo II catalytic inhibitor.

Topo II poisons such as VP16 are known to stabilize the cleavage complex that leads to DNA breaks, while catalytic inhibitors such as aclarubicin, ICRF-187, and chloroquine can protect cells against Topo II poison-induced DNA damage.[40,41] As shown in Figure 5B, Topo II poison VP16 produced a substantial increase in linear (L) DNA, indicating accumulation of the Topo IIα−DNA cleavage complex, while TSC24 had no effect in this assay, even at concentrations up to 100 μM. Moreover, VP16-induced Topo IIα−DNA cleavage complex was almost completely abated by preincubation with TSC24.

We next examined whether TSC24 induced DNA DSBs in tumor cells using the neutral single-cell gel electrophoresis assay.[42] As shown in Figure 5C, VP16 treatment caused obvious comet-shaped nuclear staining, which is the characteristic of DNA damage in cells. Consistent with the observation in Topo IIα-mediated DNA cleavage assay, TSC24 treatment did not cause any DNA damage, and pretreatment of HT-29 cells with TSC24 reversed VP16-mediated DNA DSBs. Phosphorylated histone H2A.X (γH2A.X) is an indicator of DNA DSBs which could be detected by immunostaining or Western blot.[43] As shown in Figure 4D and Figure 4E, the level of γH2A.X significantly increased after HT-29 cells were exposed to 10 μM VP16 for 1 h. TSC24 failed to induce γH2A.X, and pretreatment with TSC24 antagonized VP16-induced DNA DSBs in a concentration-dependent manner. These results are in good agreement with those obtained in the DNA cleavage assay (Figure 5B).

3.5.3. TSC24 Inhibits the Catalytic Activity of Topo IIα via Interference with Topo IIα-Mediated ATP Hydrolysis. To determine the mechanistic basis for the inhibitory action of TSC24 on Topo IIα, the effects of this compound on the individual steps of the catalytic cycle of Topo IIα were detected. Compounds that alter the gross structure of DNA by either intercalation or minor groove binding have dramatic effects on Topo II activity.[44−46] A Topo I-mediated unwinding assay was performed to test whether TSC24 could intercalate into DNA. Supercoiled DNA was relaxed by excessive Topo I in the presence of the compounds tested, and then the compounds were removed by phenol extraction following DNA relaxation. If the compound is a DNA intercalator, a new supercoiled state of DNA could be regenerated. As shown in Figure 6A, the DNA intercalator adriamycin (ADR) induced the formation of supercoiled DNA
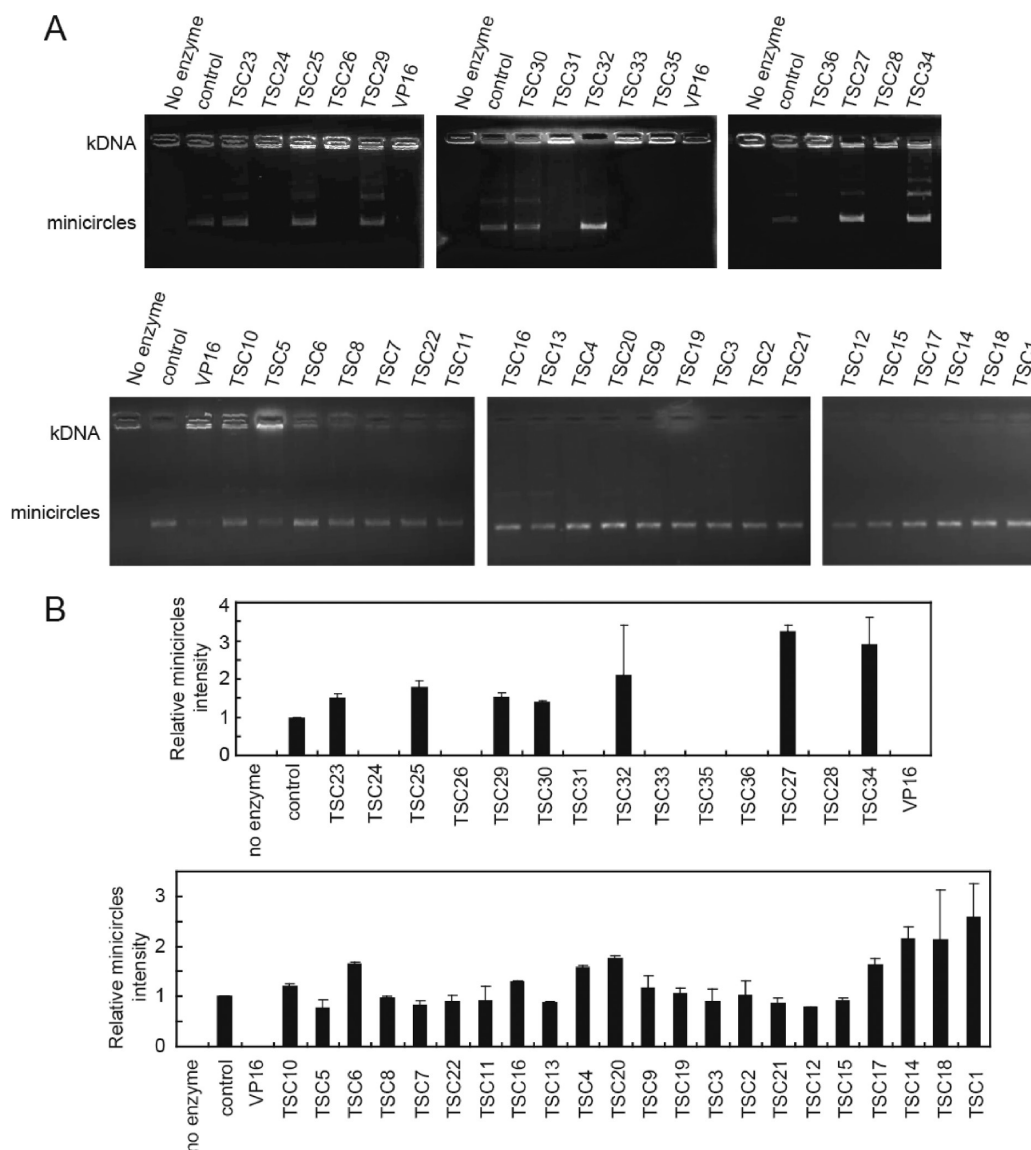
Figure 4. (A) Effects of compounds on Topo II-catalyzed kDNA decatenation. kDNA was incubated with Topo II in the presence or absence of indicated compounds (100 μM) at 37 °C for 15 min. VP16 was used as a positive control. The images of one representative experiment are shown. (B) Densitometric analysis of the data in panel A. The graphs indicate the mean $\pm$ SD of three separate experiments.

following Topo I treatment. Conversely, DNA remained relaxed in the presence of TSC24 (Figure 6A), indicating that TSC24 failed to intercalate into DNA. This result was confirmed by EB displacement experiment. The DNA-bound form of EB has a stronger fluorescence emission than free EB, so the displacement of EB from DNA could be monitored by a decrease in the fluorescence signal. As shown in Figure 6B, the fluorescence remained unchanged in the presence of TSC24, while fluorescence gradually decreased in the presence of increasing concentrations of the DNA intercalator m-AMSA, indicating that TSC24 was incapable of intercalating into DNA. To further examine whether TSC24 could bind to the minor groove of DNA, we performed a Hoechst 33258 displacement experiment. The dye Hoechst 33258 becomes brightly fluorescent upon binding to the minor groove of DNA. We found that TSC24 competitively displaced Hoechst 33258 from DNA, thus decreasing the fluorescence (Figure 6C). However, up to 100 μM TSC24 was required to reach a 58% reduction, which indicated that TSC24 was not a strong DNA minor groove binder.

The first step of the Topo II catalytic cycle is the noncovalent interaction between the enzyme and DNA. The effect of TSC24 on this initial step was detected by an electrophoretic mobility shift assay. As shown in Figure 6D, the Topo IIα−DNA complex has a slower mobility than that of free DNA in agarose gel (lanes 1 and 2). Such an upper-shift of the DNA band was abrogated in the presence of Acl because Acl prevented the binding of Topo IIα to DNA because of its DNA intercalative ability (lane 5). TSC24 had no effect on the mobility of DNA (lanes 3 and 4), indicating that TSC24 did not prevent the formation of the Topo IIα−DNA complex.

The step that immediately followed DNA binding is prestrand passage DNA cleavage. Topo II-mediated DNA strand passage requires ATP binding, so reactions in the absence of ATP represent the cleavage and relegation events that take place prior to Topo II catalyzed DNA strand passage. Unlike the overall cleavage reactions that include 1 mM ATP (Figure 5B), we carried out the prestrand passage DNA cleavage assay in the absence of ATP. As shown in
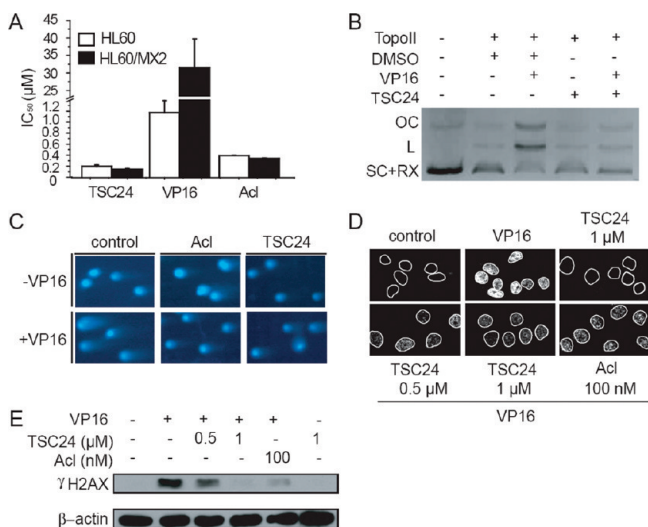
Figure 5. TSC24 acts as a catalytic inhibitor of Topo IIα. (A) TSC24 displayed similar potency against HL-60 and HL-60/MX2 cells. The graph indicates the mean ± SD from three separate experiments. (B) TSC24 antagonized VP16-trapped Topo IIα–DNA cleavage complexes. The reaction was carried out in the presence of VP16 (100 μM) with or without TSC24 (100 μM). ATP (1 mM) was included in the reactions. The positions of supercoiled DNA (SC), relaxed DNA (RX), linear DNA (L), and open-circular DNA (OC) are indicated. (C) TSC24 abrogated VP16-induced DNA double strand breaks (DSBs). HT-29 cells were pretreated with 1 μM TSC24 or 100 nM aclarubicin (Acl) for 30 min and then exposed to 10 μM VP16 for 1 h. The neutral comet assay was applied to detect DNA DSBs. (D, E) The elevation of γH2A.X was measured by immunostaining and Western blot. (D) Cells were treated as described in panel C, stained with DAPI (blue) and anti-γH2A.X antibody (green) and then examined by confocal microscopy. (E) After HT-29 cells were treated as for panel C, the level of γH2A.X was examined by Western blot. The images shown are representative of at least three independent experiments.

Figure 6E, TSC24 failed to promote DNA cleavage mediated by Topo II, whereas VP16 significantly enhanced Topo II-mediated DNA cleavage, demonstrated with an increase in the amount of linear DNA. Preincubation of TSC24 was not able to antagonize VP16-enhanced DNA cleavage in the absence of ATP, which is in contrast with the result obtained in the presence of ATP, indicating that ATP is involved in the antagonism of TSC24.

To determine whether TSC24 inhibits Topo IIα-mediated ATP hydrolysis, the human Topo IIα ATPase domain (HsATPase) was expressed using a yeast system as previously described.[34,35] The ability of HsATPase to hydrolyze ATP was measured by ATP hydrolysis assay coupled to the oxidation of NADH. As shown in Figure 6F, ATP was effectively hydrolyzed after incubation with HsATPase, which was inhibited by TSC24 in a concentration-dependent manner. Moreover, in order to demonstrate whether TSC24 inhibits ATPase activity under more physiologically relevant conditions, full-length Topo IIα was utilized in the same assay. Similar to HsATPase, the ATPase activity of full-length Topo IIα was significantly inhibited by TSC24 (Supporting Information Figure S1).

3.5.4. TSC24 Binds to the ATPase Domain of the Human Topoisomerase IIα. To shed light on how TSC24 could inhibit HsATPase-mediated ATP hydrolysis, we employed the SPR assay to test whether this effect was due to a direct interaction between TSC24 and HsATPase. The purified HsATPase was immobilized onto the hydrophilic carboxymethylated
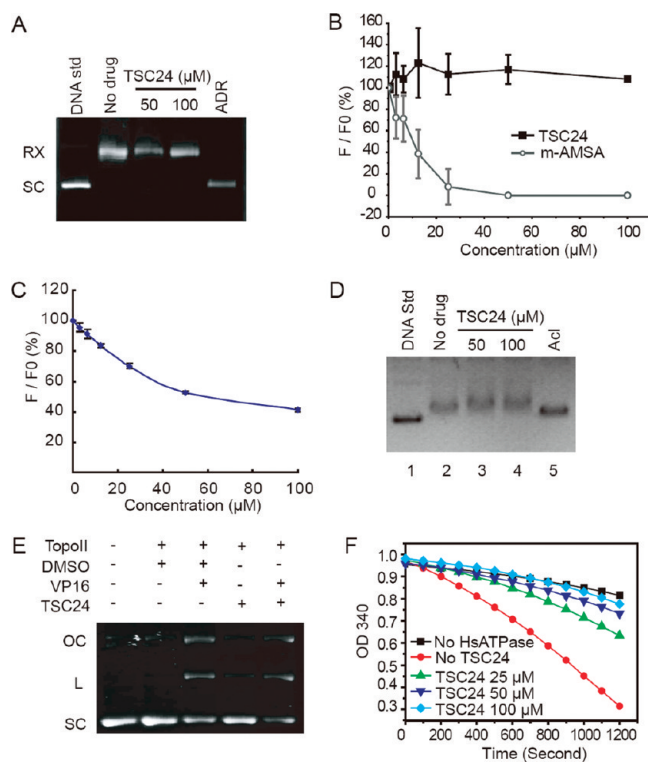

Figure 6. Effect of TSC24 on Topo IIα catalytic cycle. (A, B) TSC24 failed to intercalate into DNA. (A) Topo I-unwinding assay was performed as described in Material and Methods. (B) TSC24 did not displace EB from DNA. (C) TSC24 bound to the DNA minor groove, which was demonstrated by a Hoechst 33258 displacement experiment. (D) TSC24 had no effect on Topo IIα–DNA binding which was characterized by an electrophoretic mobility shift assay (see Material and Methods). (E) TSC24 was unable to antagonize VP16-enhanced prestrand passage DNA cleavage. The reactions were carried out in the absence of ATP. The positions of supercoiled DNA (SC), linear DNA (L), and open-circular DNA (OC) are indicated. (F) TSC24 inhibited HsATPase-mediated ATP hydrolysis in a concentration-dependent manner. The ATP hydrolysis was coupled to the oxidation of NADH, which was indicated by the decrease of the OD_{340} value. The images shown are representative of at least three independent experiments.

dextran matrix of the sensor chip CM5, and a series of buffers containing different concentrations of TSC24 or ATP were injected and flowed over the chip surface. Real-time binding sensograms were recorded. General fitting and steady-state binding affinities were calculated using BI-Aeval 3.1 software. As shown in Figure 7A, the interactions of TSC24 or ATP with HsATPase were concentration-dependent. Steady-state affinity analysis disclosed a K_D value of $(1.83 \pm 0.61) \times 10^{-5}$ M for TSC24 binding, which was lower than that for ATP ($(6.15 \pm 0.61) \times 10^{-4}$ M), indicating that TSC24 exhibited a higher affinity for HsATPase than ATP.

To explore the interaction mechanism between TSC24 and HsATPase, docking simulation was performed. As indicated in the interaction model between TSC24 and HsATPase (Figure 7B), the quinoline ring of TSC24 is positioned in the middle of the cavity, forming strong hydrophobic interactions with Asp94, Lys157, and Thr159. The N atom of the quinoline forms a hydrogen bond with the hydroxyl group of Ser 149. The thiosemicarbazone moiety points to the entrance of the active pocket, and an N atom in this moiety undergoes a strong hydrogen bond interaction with the side chain NH of Lys 157. To test the docking prediction, we
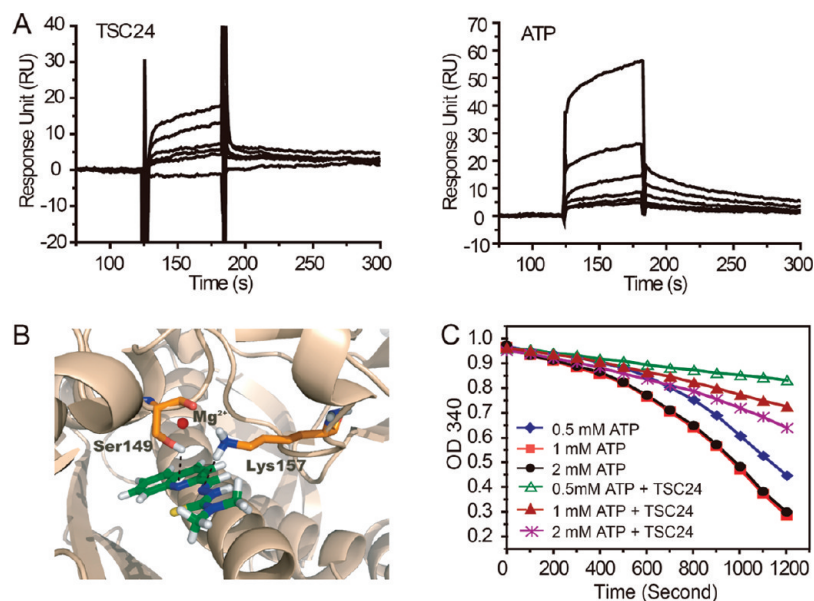
Figure 7. TSC24 binds to the ATPase domain of Topo IIα. (A) The interaction between TSC24 and ATP with immobilized HsATPase was measured by surface plasmon resonance spectroscopy (SPR). The concentration series from top to bottom are 100, 50, 25, 12.5, 6.25, 3.125 μM for TSC24 (left) and 2, 1, 0.5, 0.25, 0.125, 0.0625 mM for ATP (right). (B) Molecular docking predicted that TSC24 might bind to the ATP binding pocket of human Topo IIα. The dashed lines represent the hydrogen bonds between TSC24 and residues in the ATP binding site of human Topo IIα. The red ball represents Mg^{2+}. The pictures were prepared using the PyMol programs (http://pymol.sourceforge.net/). (C) Inhibition of TSC24 on HsATPase-catalyzed ATP hydrolysis was dependent on the concentration of ATP. Data shown are representative of at least three independent experiments.

performed a competitive inhibition assay to investigate the effect of different concentrations of ATP on the TSC24-mediated inhibition of ATP hydrolysis. As shown in Figure 7C, there was no obvious difference in the ATP hydrolysis activity in the presence of 1 or 2 mM ATP, indicating that the enzyme had been saturated with ATP. However, increased concentrations of ATP resulted in weaker inhibitory activity of TSC24 on HsATPase-mediated ATP hydrolysis (Figure 7C), suggesting that TSC24 functioned as an ATP competitor.

4. Discussion

We designed and prepared a class of novel α-heterocyclic carboxaldehyde TSCs, which were synthesized by introducing condensed heterocycles at the N^1 position. Among them, five compounds were found to possess potent cytotoxic activity against a panel of four human tumor cell lines, in which TSC24 was selected for further evaluation and mechanistic study because of its distinguished antiproliferative activity. TSC24 exhibited broad antiproliferative activites against a wide variety of tumor cells originating from different tissue types. Of particular note, TSC24 was more potent against multidrug resistant cells than against their corresponding parental cells. The anticancer activity of TSC24 is further supported by the observation that TSC administration significantly repressed tumor growth in mice bearing S-180 sarcoma. Therefore, TSC24 represents a class of novel TSCs possessing profound anticancer potency. Studies on the structure−activity relationship and its mode of action were conducted in this report.

4.1. Structure−Activity Relationship (SAR). SAR exploration first focused on the N^4 portion of the molecule and their anticancer activities. Twenty-two compounds (TSC1−TSC22) showed IC$_{50}$ values in the micromolar range. Compound TSC1, having a phenyl substitution at the N^4 position, displayed moderate antiproliferative activity with IC$_{50}$

values ranging from 9.13 to 27.39 μM against different cell lines. Replacement of the phenyl group of TSC1 with methoxyphenyl groups (TSC2−TSC4) gave a 5-fold loss of potency. Methylphenyl group-substituted compounds TSC6 and TSC7 were also examined and found to be less potent than TSC2−TSC5. Additionally, a dramatic loss of antiproliferative activity was observed for the semicarbazide TSC8, indicating that the sulfur atom is important for potency. Halogenated phenyl groups placed at the para- or meta-position (TSC10−TSC13, TSC15, and TSC16) caused an approximate potency in comparison with TSC1. However, shifting the halogen atoms to the ortho-positions (TSC9 and TSC14) was not tolerated. Interestingly, introduction of a 2-trifluoromethylphenyl group at the N^4 position gave equivalent activity to TSC1. Further substitution of the phenyl group with 4-cyano TSC19 and 2,6-diisopropyl TSC20 resulted in moderate antiproliferative activity with IC$_{50}$ values lower than 25 μM against all of the selected cell lines. Truncation of the aryl moiety attach to the N^4 atom to give the compound TSC23 resulted in significant loss of activity. Smaller alkyl groups, however, were well tolerated. Replacement of the hydrogen atoms at the N^4 position with methyl groups (TSC24) resulted in significant increases in potency. SAR around the N^4 position appeared to be tightly constrained. Thus, we turned our attention to the aldehyde portion of the molecule. Quinolin-2-ylmethylene substitution at the N^1 position, TSC24, resulted in the most potent activity with an IC$_{50}$ of 0.02 μM against the HT-29 cell line. However, substitution with quinoxalin-2-ylmethylene and 1,8-naphthyridin-2-(yl)methylene gave compounds TSC26 and TSC28, respectively, with an approximately 2- to 19-fold drop in potency in comparison with TSC24. The steric limitations of these two compounds are similar; loss of activity is presumably due to the electronic properties of the diverse condensed heteroaromatic core structures. Moreover, the benzo[*d*]thiazol-2-ylmethylene and benzo[*b*]thiophen-2-ylmethylene substituted derivatives TSC31 and TSC33, respectively, revealed

an obvious loss of antiproliferative activity. This finding demonstrated the importance of the six-member heterocycle attached to the methylene for potency. The benzo[*h*][1,6]-naphthyridin-5-ylmethylene substituted derivative TSC36 was among the most potent compounds and displayed IC_{50} values in the range $0.04-1.72$ μM.

4.2. TSC24 Exerts Its Antitumor Activities through Inhibition of Topo IIα Catalytic Activity in Addition to Iron Chelating. Similar to other reported TSCs, TSC24 could chelate Fe in tumor cells, which resulted in the inhibition of DNA synthesis and cell cycle arrest at the G1/S boundary, indicating that its ability to chelate Fe contributes to its antiproliferative activity. However, TSC24 inhibited DNA synthesis with an IC_{50} of 0.36 μM, which was much higher than that for the inhibition of cell proliferation (0.02 μM). In contrast to TSC24, the concentrations for HU and DFO to inhibit DNA synthesis and cell proliferation are very similar, indicating that inhibition of DNA synthesis by Fe chelation may not be responsible alone for TSC24 to exert its antiproliferative activity. Furthermore, supplementation of Fe increased the IC_{50} of TSC24 against HT-29 cells by about 3-fold, while the IC_{50} of DFO increased about 8-fold under the same conditions, indicating that other mechanisms might also be involved in the antitumor activity of TSC24. We performed a COMPARE analysis to predict the possible mechanism for TSC derivatives and found a mechanistic similarity between TSC derivatives and Topo II inhibitors. The COMPARE algorithm is a Web-based platform to compare the similarity of the antiproliferative profiles of a specific "seed" compound to the patterns of 175 standard agents with known mechanisms of action. It has been successfully used to predict mechanisms for a wide variety of compounds, such as the identification of MAP-kinase-kinase as a substrate for anthrax lethal factor (NSC678519).[47] By this analysis, we revealed that Topo II inhibitors were among the compounds whose antiproliferative profiles were most positively correlated to TSC derivatives tested. Moreover, sporadic studies also indicated that TSC derivatives acted as Topo II inhibitors.[16,36] More recently, Rao et al. reported TSC derivative Dp44mT inhibited Topo IIa as our manuscript was in preparation.[48] In accordance with this prediction, we confirmed that TSC24 directly inhibited the catalytic activity of Topo IIα in a series of experiments.

Topo II is an essential enzyme that participates in various DNA metabolic processes such as transcription, replication, recombination, and chromosome condensation and decondensation. Topo II has been identified as a clinically important target for cancer chemotherapy, and Topo II poisons are central components in many therapeutic regimens.[49] In this study, we found that TSC24 markedly inhibited Topo IIα-catalyzed supercoiled DNA relaxation and kDNA decatenation in a cell-free system. TSC24 also inhibited Topo II in cells, and this action contributed to its anticancer activity based on the following evidence. First, inhibitory activities of a series of TSC compounds against Topo II are positively correlated with their antiproliferative activities in cells; i.e., compounds displaying superior activity against Topo II are more potent to inhibit tumor cell proliferation (Figure 4 and Table 1). Second, pretreatment of cells with TSC24 could block VP16-induced DNA DSBs in cells. This is one of the typical properties of Topo II catalytic inhibitors. Moreover, the concentration of TSC 24 to block VP16-induced DNA damage is in the pharmacological range. Third, TSC24 arrested synchronized cells at the M phase and the concentration was similar to that of chelating iron in cells (Figure 3D). Other iron chelators such as

DFO and 3-AP could not induce cell cycle arrest at the M phase, so arresting synchronized cells at the M phase by TSC24 is not due to chelating iron. Instead, inhibition of Topo II that has essential roles in sister chromatid separation at anaphase could result in M phase arrest. Therefore, although we could not rule out other mechanisms, it is likely that TSC24 arrests cell cycle at the M phase via inhibition of Topo II in cells.

Meanwhile, we notice that the concentration of TSC24 required to appreciably inhibit Topo II appears to be considerably higher than that required to inhibit cell proliferation, which might be due to the following two reasons. First, both Topo II inhibition and iron chelation combinatorially contributed to the antiproliferative activity of TSC24. Second, the concentration required to inhibit Topo II activity in purified enzyme assay is usually much higher than that in a cell proliferation assay. It might be owing to the different sensitivity between different experimental systems as well as signal cascade in which partial inhibition may elicit enlarged response in cells.

4.3. TSC24 Competes with ATP To Bind to the ATPase Domain of Human Topoisomerase IIα. Topo II inhibitors are commonly classified as poisons and catalytic inhibitors. Topo II poisons stabilize the enzyme−DNA intermediate (also known as the cleavage complex), whereas catalytic inhibitors may act at any of the other steps in the catalytic cycles. Although Topo II poisons are currently widely used in the clinical treatment of human malignancies, the development of Topo II catalytic inhibitors attracts continuous interest, with the aim of modulating the cytotoxic effects of Topo II poisons[40,41,50] and overcoming at-MDR.[51,52] Our present study established TSC24 as a catalytic inhibitor based on the following evidence. First, HL-60/MX2 cells, which are resistant to Topo II poison such as VP16 were fully sensitive to TSC24. Second, TSC24 failed to trap Topo IIα−DNA complexes but antagonized VP16-stabilized cleavage complexes in the presence of ATP. Finally, TSC24 was unable to induce DNA damage but abrogated VP16-mediated DNA damage in HT-29 cells.

Topo II catalytic inhibitors are a heterogeneous group of compounds that might interfere with DNA−Topo II binding (aclarubicin and suramin),[44] block DNA cleavage (merbarone),[53] or inhibit ATP binding (novobiocin).[54,55] By dissecting the actions of TSC24 on the individual steps of the Topo IIα catalytic cycle, we found that TSC24 had a weak affinity for DNA minor groove. However, since TSC24 could neither prevent the formation of Topo II−DNA complex nor inhibit Topo I-mediated pBR322 relaxation, we assume that the ability of TSC24 to bind to DNA minor groove may not be strong enough to alter the gross structure of DNA or to interfere with the catalytic activity of topoisomerase. Topo II is an ATP-dependent enzyme, while the catalytic activity of Topo I does not require ATP. We further found that TSC24 inhibited Topo II-mediated ATP hydrolysis, which explains why TSC24 inhibits the catalytic activity of Topo II while it spares Topo I.

Data from the SPR assay showed that TSC24 exhibited high affinity for HsATPase. Several well-known Topo II catalytic inhibitors have been reported to directly bind to the ATPase domain of Topo II; bisdioxopiperazines, such as ICRF-187, do not compete for the ATP-binding pocket in ATPase domain but rather bridge and stabilize a transient dimer interface between two ATPase subunits.[56] Furthermore, coumarins, such as novobiocin, interact with DNA gyrase B and compete with ATP binding.[54] Molecular docking predicted that TSC24 bound to the ATP-binding pocket

of human Topo IIα. Consistently, increased concentrations of ATP weakened the inhibition of HsATPase-catalyzed ATP hydrolysis by TSC24, suggesting that TSC24 acts as an ATP competitor like novobiocin. Therefore, TSC24 was unable to block VP16-enhanced DNA cleavage in the absence of ATP. However, we cannot rule out the possible involvement of other domains of Topo IIα in the TSC24-mediated inhibition of Topo IIα catalytic activity. These results disclosed a different mechanism from the action of the iron chelator Dp44mT, which was reported recently as a Topo IIα poison.[48]

In conclusion, we reported a series of novel TSC derivatives bearing condensed heterocyclic carboxaldehyde moieties that possessed potent anticancer activity and for the first time dissected the mechanism to inhibit Topo II. Thirty-six derivatives were synthesized, and five of them exhibited potent antiproliferative activity. In addition, the most active compound TSC24 was selected for further evaluation and mechanism research at molecular and cellular levels. The results indicated that TSC24 exerts its antitumor activities through inhibition of Topo IIα catalytic activity in addition to iron chelation. Moreover, we elucidate for the first time that TSC24 acts as a Topo II catalytic inhibitor via binding to the ATPase domain of Topo IIα and inhibition of Topo IIα-mediated ATP hydrolysis. Mechanistic studies of TSC24 will provide insights into the discovery and development of new TSC derivatives and Topo II inhibitors.

5. Experimental Section

5.1. Chemistry. The reagents (chemicals) were purchased from commercial sources. Analytical thin layer chromatography (TLC) was done with HSGF 254 plates (0.15−0.2 mm thickness). All products were characterized by their NMR and MS spectra. NMR spectra were performed on Bruker AMX-400 and AMX-300 NMR spectrometers (using tetramethylsilane as an internal standard). Chemical shifts were reported in parts per million (ppm, δ) downfield from tetramethylsilane. Proton coupling patterns were described as singlet (s), doublet (d), triplet (t), quartet (q), multiplet (m), and broad (br). Low- and high-resolution mass spectra (LRMS and HRMS) were measured on a Finnigan MAT 95 spectrometer. All of the microwave-assistant reactions were performed in an Initiator EXP microwave system (Biotage, Inc.) at the specified temperature using the standard mode of operation. For the targeted compounds the chemical purity was determined using the following conditions: an Agilent 1100 series HPLC with an Agilent Zorbax Eclipse XDB- C$_{18}$ (4.6 mm × 50 mm, 5 μm) reversed phase column; method I, CH$_3$OH/H$_2$O, 65% (v/v) of CH$_3$OH gradient, flow rate of 0.6 mL/min, λ = 280 nm; method II, CH$_3$CN/H$_2$O, 70%(v/v) of CH$_3$CN gradient, flow rate of 0.6 mL/min, λ = 280 nm. The purity of each compound was ≥95% in either analysis.

5.1.1. General Procedure for the Synthesis of Thiosemicarbazones B1−B22. To a stirred solution of hydrazine hydrate (85%, 2.4 mmol) in 20 mL of isopropanol, iso(thio)cyanate (2.0 mmol) was added at room temperature. Precipitate was formed immediately. Stirring was continued for 30 min. Then the mixture was filtered and the precipitate was washed with isopropanol three times to give intermediate **B**.

5.1.2. General Procedure for the Synthesis of α-Heterocyclic Carboxaldehyde Thiosemicarbazones TSC1-TSC22 (Method A). To a stirred solution of **B** (1 mmol) in 15 mL of isopropanol, quinoline-2-carbaldehyde (1.2 mmol) and a drop of acetic acid were added at room temperature. Stirring was continued for 2 h. Then the mixture was filtered and the precipitate was washed with isopropanol three times to give the crude product. Then the

crude product was purified through preparative RP-HPLC to afford α-heterocyclic carboxaldehyde TSCs.

5.1.3. General Procedure for the Synthesis of α-Heterocyclic Carboxaldehyde Thiosemicarbazones TSC24-TSC36 (Method B). The α-heterocyclic carboxaldehyde (0.3 mmol) was suspended in 2-propanol (4 mL) in a 10 mL glass vial equipped with a small magnetic stirring bar. To this was added an equimolar quantity of thiosemicarbazide, and the vial was tightly sealed with an aluminum/Teflon crimp top. The mixture was then irradiated for 25 min at 100 °C. After completion of the reaction, the vial was cooled to 50 °C by air jet cooling before it was opened. The precipitated product was collected by filtration and washed with cold 2-propanol to furnish α-heterocyclic carboxaldehyde TSC as a solid. Pure samples were obtained by additional recrystallization from methanol/2-propanol.

N-Phenylhydrazinecarbothioamide (**B1**). Yield: 97%. ^{1}H NMR (300 MHz, DMSO-d_6): δ 9.14 (s, 1H), 7.65−7.63 (m, 1H), 7.32−7.26 (m, 3H), 7.11−7.06 (m, 1H), 4.80−4.77 (br, 2H).

N-(2-Methoxyphenyl)hydrazinecarbothioamide (**B2**). Yield: 89%. ^{1}H NMR (300 MHz, DMSO-d_6): δ 9.96 (br, 1H), 9.23 (s, J = 8.4 Hz, 1H), 8.75 (d, J = 4.5 Hz, 1H), 7.08−6.87 (m, 3H), 4.86 (br, 2H), 3.84 (s, 3H).

N-(3-Methoxyphenyl)hydrazinecarbothioamide (**B3**). Yield: 88%. ^{1}H NMR (300 MHz, DMSO-d_6): δ 9.16 (s, 1H), 7.48 (s, 1H), 7.20−7.15 (m, 2H), 6.68−6.64 (m, 1H), 3.73 (s, 3H).

N-(4-Methoxyphenyl)hydrazinecarbothioamide (**B4**). Yield: 70%. ^{1}H NMR (DMSO-d_6): δ 8.99 (s, 1H), 7.43 (d, J = 4.5 Hz, 2H), 6.88−6.84 (m, 2H), 3.73 (s, 3H).

N-*o*-Tolylhydrazinecarbothioamide (**B5**). Yield: 95%. ^{1}H NMR (300 MHz, DMSO-d_6): δ 9.06 (s, 1H), 7.53 (s, 1H), 7.21−7.06 (m, 3H), 2.19 (s, 3H).

N-*m*-Tolylhydrazinecarbothioamide (**B6**). Yield: 90%. ^{1}H NMR (300 MHz, DMSO-d_6): δ 9.10 (s, 1H), 7.45 (s, 2H), 7.17 (t, J = 16 Hz, 1H), 6.91 (d, J = 7.5 Hz, 1H), 2.28(s, 3H).

N-*p*-Tolylhydrazinecarbothioamide (**B7**). Yield: 92%. ^{1}H NMR (300 MHz, DMSO-d_6): δ 9.06 (s, 1H), 7.48 (d, J = 6.0 Hz, 2H), 7.09 (d, J = 6.0 Hz, 2H), 2.49 (s, 3H).

N-*p*-Tolylhydrazinecarboamide (**B8**). Yield: 90%. ^{1}H NMR (300 MHz, DMSO-d_6): δ 8.50 (s, 1H), 7.39−7.01 (m, 4H), 2.21 (s, 3H).

N-(2-Fluorophenyl)hydrazinecarbothioamide (**B9**). Yield: 93%. ^{1}H NMR (DMSO-d_6): δ 9.36 (s, 1H), 8.07−8.02 (m, 1H), 7.27−7.11 (m, 3H).

N-(3-Fluorophenyl)hydrazinecarbothioamide (**B10**). Yield: 88%. ^{1}H NMR (DMSO-d_6): δ 9.30 (s, 1H), 7.86 (d, J = 6.0 Hz, 1H), 7.46−7.27 (m, 2H), 6.93−6.88 (m, 1H).

N-(4-Fluorophenyl)hydrazinecarbothioamide (**B11**). Yield: 90%. ^{1}H NMR (DMSO-d_6): δ 9.14 (s, 1H), 7.62−7.58 (m, 2H), 7.15−7.09 (m, 2H).

N-(3-Chlorophenyl)hydrazinecarbothioamide (**B12**). Yield: 85%. ^{1}H NMR (DMSO-d_6): δ 9.31 (s, 1H), 7.99 (s, 1H), 7.58−7.56 (m, 1H), 7.30 (t, J = 8.4 Hz, 1H), 7.15−7.12 (m, 1H).

N-(4-Chlorophenyl)hydrazinecarbothioamide (**B13**). Yield: 90%. ^{1}H NMR (DMSO-d_6): δ 9.24 (s, 1H), 7.70−7.68 (m, 2H), 7.36−7.32 (m, 2H).

N-(2-Bromophenyl)hydrazinecarbothioamide (**B14**). Yield: 94%. ^{1}H NMR (300 MHz, DMSO-d_6): δ 9.44 (s, 1H), 8.38−8.36 (m, 1H), 7.66−7.62 (m, 1H), 7.38−7.32 (m, 1H), 7.11−7.05 (m, 1H).

N-(3-Bromophenyl)hydrazinecarbothioamide (**B15**). Yield: 88%. ^{1}H NMR (300 MHz, DMSO-d_6): δ 9.27 (s, 1H), 8.11 (s, 1H), 7.60 (s, 1H), 7.26−7.21 (m, 2H).

N-(4-Bromophenyl)hydrazinecarbothioamide (**B16**). Yield: 66%. ^{1}H NMR (300 MHz, DMSO-d_6): δ 9.20 (br, 1H), 7.66−7.64 (m, 2H), 7.47−7.46 (m, 2H).

N-(2-(Trifluoromethyl)phenyl)hydrazinecarbothioamide (**B17**). Yield: 91%. ^{1}H NMR (300 MHz, DMSO-d_6): δ 9.49 (s, 1H), 8.05 (d, J = 6.0 Hz, 1H), 7.71−7.62 (m, 2H), 7.37 (t, J = 7.8 Hz, 1H).

N-(4-(Trifluoromethyl)phenyl)hydrazinecarbothioamide (**B18**). Yield: 91%. ^{1}H NMR (300 MHz, DMSO-d_6): δ 9.41 (s, 1H), 7.98 (d, J = 6.0 Hz, 2H), 7.64 (d, J = 4.2 Hz, 2H).

N-(4-Cyanophenyl)hydrazinecarbothioamide (B19). Yield: 91%. ^{1}H NMR (300 MHz, DMSO-d_6): δ 9.24 (s, 1H), 7.86−7.79 (m, 2H), 7.43−7.39 (m, 2H).

N-(2,6-Diisopropylphenyl)hydrazinecarbothioamide (B20). Yield: 72%. ^{1}H NMR (300 MHz, DMSO-d_6): δ 7.25−7.10 (m, 3H), 4.75 (br, 2H), 3.08−2.98 (m, 2H), 1.07 (dd, J = 11.4 Hz, 6.9 Hz, 12H).

N-(2-Methoxy-5-methylphenyl)hydrazinecarbothioamide (B21). Yield: 95%. ^{1}H NMR (300 MHz, DMSO-d_6): δ 9.92 (br, 1H), 9.18 (s, 1H), 8.62 (br, 1H), 6.93−6.82 (m, 2H), 4.84 (br, 1H), 3.80 (s, 3H), 2.22 (s, 3H).

N-Benzylhydrazinecarbothioamide (B22). Yield: 93%. ^{1}H NMR (DMSO-d_6): δ 8.76 (s, 1H), 8.30 (br, 1H), 7.31−7.20 (m, 5H), 4.71 (d, J = 6.0 Hz, 2H).

N-Phenyl-2-(quinolin-2-ylmethylene)hydrazinecarbothioamide (TSC1). TSC1 was prepared from **B1** according to general procedure (method A). Yield: 70%. ^{1}H NMR (300 MHz, DMSO-d_6): δ 12.21 (s, 1H), 10.41 (s, 1H), 8.64 (d, J = 8.4 Hz, 1H), 8.41 (d, J = 9.0 Hz, 1H), 8.35 (s, 1H), 8.03 (t, J = 8.7 Hz, 2H), 7.83−7.77 (m, 1H), 7.67−7.56 (m, 3H), 7.42 (t, J = 7.5 Hz, 2H), 7.26 (t, J = 7.5 Hz, 1H). MS (EI, m/z): 306 [M]$^+$. HRMS (EI): calcd for $C_{17}H_{14}N_4S$ [M]$^+$, 306.0939; found 306.0932.

N-(2-Methoxyphenyl)-2-(quinolin-2-ylmethylene)hydrazinecarbothioamide (TSC2). TSC2 was prepared from **B2** according to general procedure (method A). Yield: 61%. ^{1}H NMR (300 MHz, DMSO-d_6): δ 12.24 (s, 1H), 10.13 (s, 1H), 8.60 (d, J = 8.1 Hz, 1H), 8.40 (d, J = 8.4 Hz, 1H), 8.30 (s, 1H), 8.03 (t, J = 9.0 Hz, 2H), 7.88−7.76 (m, 2H), 7.64−7.60 (m, 2H), 7.12−7.10 (m, 1H), 6.99−6.95 (m. 1H), 3.88 (s, 3H). MS (EI, m/z): 336 [M]$^+$. HRMS (EI): calcd for $C_{18}H_{16}N_4OS$ [M]$^+$, 336.1045; found 336.1044.

N-(3-Methoxyphenyl)-2-(quinolin-2-ylmethylene)hydrazinecarbothioamide (TSC3). TSC3 was prepared from **B3** according to general procedure (method A). Yield: 44%. ^{1}H NMR (300 MHz, DMSO-d_6): δ 12.22 (s, 1H), 10.35 (s, 1H), 8.63 (d, J = 8.4 Hz, 1H), 8.41 (d, J = 8.7 Hz, 1H), 8.40 (s, 1H), 8.03 (t, J = 9.0 Hz, 2H), 7.83−7.77 (m, 1H), 7.67−7.62 (m, 1H), 7.34−7.18 (m, 3H), 6.86−6.82 (m, 1H), 3.78 (s, 3H). MS (EI, m/z): 336 [M]$^+$. HRMS (EI): calcd for $C_{18}H_{16}N_4OS$ [M]$^+$, 336.1045; found 336.1036.

N-(4-Methoxyphenyl)-2-(quinolin-2-ylmethylene)hydrazinecarbothioamide (TSC4). TSC4 was prepared from **B4** according to general procedure (method A). Yield: 59%. ^{1}H NMR (300 MHz, DMSO-d_6): δ 12.14 (s, 1H), 10.31 (s, 1H), 8.64 (d, J = 8.7 Hz, 1H), 8.40 (d, J = 8.4 Hz, 1H), 8.33 (s, 1H), 8.02 (t, J = 8.4 Hz, 2H), 7.82−7.77 (m, 1H), 7.66−7.61 (m, 1H), 7.41 (t, J = 6.9 Hz, 2H), 6.97 (t, J = 6.9 Hz, 2H), 3.78 (s, 3H). MS (EI, m/z): 336 [M]$^+$. HRMS (EI): calcd for $C_{18}H_{16}N_4OS$ [M]$^+$, 336.1045; found 336.1045.

N-(2-Methylphenyl)-2-(quinolin-2-ylmethylene)hydrazinecarbothioamide (TSC5). TSC5 was prepared from **B5** according to general procedure (method A). Yield: 47%. ^{1}H NMR (300 MHz, DMSO-d_6): δ 12.18 (s, 1H), 10.28 (s, 1H), 8.63 (d, J = 6.0 Hz, 1H), 8.38 (d, J = 4.5 Hz, 1H), 8.33 (s, 1H), 7.78 (m, 1H), 7.65 (m, 1H), 7.32−7.24 (m, 4H), 2.27 (s, 1H). MS (EI, m/z): 320 [M]$^+$. HRMS (EI): calcd for $C_{18}H_{16}N_4S$ [M]$^+$, 320.1096; found 320.1101.

N-(3-Methylphenyl)-2-(quinolin-2-ylmethylene)hydrazinecarbothioamide (TSC6). TSC6 was prepared from **B6** according to general procedure (method A). Yield: 53%. ^{1}H NMR (300 MHz, DMSO-d_6): δ 11.14 (s, 1H), 9.06 (s, 1H), 8.55 (d, J = 6.0 Hz, 1H), 8.41 (d, J = 4.5 Hz, 1H), 8.14 (s, 1H), 8.03−8.00 (m, 1H), 7.79−7.78 (m, 1H), 7.66−7.56 (m, 3H), 7.14 (d, J = 4.5 Hz, 1H). MS (EI, m/z): 320 [M]$^+$. HRMS (EI): calcd for $C_{18}H_{16}N_4S$ [M]$^+$, 320.1096; found 320.1092.

N-(4-Methylphenyl)-2-(quinolin-2-ylmethylene)hydrazinecarbothioamide (TSC7). TSC7 was prepared from **B7** according to general procedure (method A). Yield: 44%. ^{1}H NMR (300 MHz, DMSO-d_6): δ 12.16 (s, 1H), 10.33 (s, 1H), 8.61 (d, J = 6.0 Hz, 1H), 8.37 (d, J = 6.0 Hz, 1H), 8.31 (s, 1H), 8.02−7.97 (m, 2H), 7.78−7.74 (m, 1H), 7.63−7.59 (m, 1H), 7.40−7.38 (m, 2H),

7.20−7.18 (d, J = 3.0 Hz, 1H), 2.31 (s, 3H). MS (EI, m/z): 320 [M]$^+$. HRMS (EI): calcd for $C_{18}H_{16}N_4S$ [M]$^+$, 320.1096; found 320.1104.

N-(4-Methylphenyl)-2-(quinolin-2-ylmethylene)hydrazinecarboamide (TSC8). TSC8 was prepared from **B8** according to general procedure (method A). Yield: 55%. ^{1}H NMR (300 MHz, DMSO-d_6): δ 11.14 (s, 1H), 9.05 (s, 1H), 8.55 (d, J = 6.0 Hz, 1H), 8.41 (d, J = 4.5 Hz, 1H), 8.14 (s, 1H), 8.03−7.99 (m, 1H), 7.79−7.77 (m, 1H), 7.66−7.56 (m, 3H), 7.14 (d, J = 4.5 Hz, 1H). MS (EI, m/z): 304 [M]$^+$. HRMS (EI): calcd for $C_{18}H_{16}N_4O$ [M]$^+$, 304.1324; found 304.1332.

N-(2-Fluorophenyl)-2-(quinolin-2-ylmethylene)hydrazinecarbothioamide (TSC9). TSC9 was prepared from **B9** according to general procedure (method A). Yield: 47%. ^{1}H NMR (300 MHz, DMSO-d_6): δ 12.34 (s, 1H), 10.26 (s, 1H), 8.57 (d, J = 4.5 Hz, 1H), 8.38 (d, J = 4.5 Hz, 1H), 8.31 (s, 1H), 8.03−7.97 (m, 2H), 7.77−7.75 (m, 1H), 7.64−7.62 (m, 1H), 7.47−7.46 (m, 1H), 7.35−7.23 (m, 2H). MS (EI, m/z): 324 [M]$^+$. HRMS (EI): calcd for $C_{17}H_{13}FN_4S$ [M]$^+$, 324.0845; found 324.0844.

N-(3-Fluorophenyl)-2-(quinolin-2-ylmethylene)hydrazinecarbothioamide (TSC10). TSC10 was prepared from **B10** according to general procedure (method A). Yield: 41%. ^{1}H NMR (300 MHz, DMSO-d_6): δ 12.33 (s, 1H), 10.45 (s, 1H), 8.65 (d, J = 4.5 Hz, 1H), 8.43 (d, J = 9.0 Hz, 1H), 8.36 (s, 1H), 8.03 (t, J = 9.0 Hz, 2H), 7.79 (t, J = 6.0 Hz, 1H), 7.67−7.57 (m, 2H), 7.47−7.44 (m, 2H), 7.10−7.09 (m, 1H). MS (EI, m/z): 324 [M]$^+$. HRMS (EI): calcd for $C_{17}H_{13}FN_4S$ [M]$^+$, 324.0845; found 324.0848.

N-(4-Fluorophenyl)-2-(quinolin-2-ylmethylene)hydrazinecarbothioamide (TSC11). TSC11 was prepared from **B11** according to general procedure (method A). Yield: 40%. ^{1}H NMR (300 MHz, DMSO-d_6): δ 12.24 (s, 1H), 10.40 (s, 1H), 8.63 (d, J = 4.5 Hz, 1H), 8.42 (d, J = 6.0 Hz, 1H), 8.35 (s, 1H), 8.03 (t, J = 9.0 Hz, 2H), 7.83−7.78 (m, 1H), 7.67−7.54 (m, 3H), 7.25 (t, J = 9.0 Hz, 2H). MS (EI, m/z): 324 [M]$^+$. HRMS (EI): calcd for $C_{17}H_{13}FN_4S$ [M]$^+$, 324.0845; found 324.0840.

N-(3-Chlorophenyl)-2-(quinolin-2-ylmethylene)hydrazinecarbothioamide (TSC12). TSC12 was prepared from **B12** according to general procedure (method A). Yield: 46%. ^{1}H NMR (300 MHz, DMSO-d_6): δ 12.34 (s, 1H), 10.45 (s, 1H), 8.62 (d, J = 8.7 Hz, 1H), 8.43 (d, J = 9.0 Hz, 1H), 8.36 (s, 1H), 8.06−8.00 (m, 2H), 7.83−7.74 (m, 2H), 7.67−7.60 (m, 2H), 7.47−7.42 (m, 1H), 7.34−7.30 (m, 1H), MS (EI, m/z): 340 [M]$^+$. HRMS (EI): calcd for $C_{17}H_{13}ClN_4S$ [M]$^+$, 340.0549; found 340.0558.

N-(4-Chlorophenyl)-2-(quinolin-2-ylmethylene)hydrazinecarbothioamide (TSC13). TSC13 was prepared from **B13** according to general procedure (method A). Yield: 49%. ^{1}H NMR (300 MHz, DMSO-d_6): δ 12.28 (s, 1H), 10.41 (s, 1H), 8.59 (d, J = 6.0 Hz, 1H), 8.39 (d, J = 6.0 Hz, 1H), 8.32 (s, 1H), 8.03−7.97 (m, 2H), 7.79−7.75 (m, 1H), 7.64−7.58 (m, 3H), 7.47−7.44 (m, 2H). MS (EI, m/z): 340 [M]$^+$. HRMS (EI): calcd for $C_{17}H_{13}ClN_4S$ [M]$^+$, 340.0549; found 340.0548.

N-(2-Bromophenyl)-2-(quinolin-2-ylmethylene)hydrazinecarbothioamide (TSC14). TSC14 was prepared from **B14** according to general procedure (method A). Yield: 44%. ^{1}H NMR (300 MHz, DMSO-d_6): δ 12.37 (s, 1H), 10.31 (s, 1H), 8.50 (d, J = 6.3 Hz, 1H), 8.38 (d, J = 6.6 Hz, 1H), 8.32 (s, 1H), 8.03−7.96 (m, 2H), 7.80−7.72 (m, 3H), 7.64−7.55 (m, 3H). MS (EI, m/z): 324 [M]$^+$. HRMS (EI): calcd for $C_{17}H_{13}BrN_4S$ [M]$^+$, 384.0044; found 383.9959.

N-(3-Bromophenyl)-2-(quinolin-2-ylmethylene)hydrazinecarbothioamide (TSC15). TSC15 was prepared from **B15** according to general procedure (method A). Yield: 56%. ^{1}H NMR (300 MHz, DMSO-d_6): δ 12.32 (s, 1H), 10.43 (s, 1H), 8.61 (d, J = 8.7 Hz, 1H), 8.41 (d, J = 8.7 Hz, 1H), 8.35 (s, 1H), 8.02 (t, J = 9.0 Hz, 2H), 7.86−7.74 (m, 1H), 7.66−7.61 (m, 2H), 7.46−7.34 (m, 2H). MS (EI, m/z): 384 [M]$^+$. HRMS (EI): calcd for $C_{17}H_{13}BrN_4S$ [M]$^+$, 384.0044; found 384.0029.

N-(4-Bromophenyl)-2-(quinolin-2-ylmethylene)hydrazinecarbothioamide (TSC16). TSC16 was prepared from **B16** according to general procedure (method A). Yield: 52%. ^{1}H NMR

(300 MHz, DMSO-d_6): δ 12.28 (s, 1H), 10.40 (s, 1H), 8.60 (d, $J = 8.4$ Hz, 1H), 8.40 (d, $J = 8.7$ Hz, 1H), 8.34 (s, 1H), 8.02 (t, $J = 8.7$ Hz, 2H), 7.81−7.76 (m, 2H), 7.66−7.54 (m, 5H). MS (EI, *m/z*): 384 [M]$^+$. HRMS (EI): calcd for C$_{17}$H$_{13}$BrN$_4$S [M]$^+$, 384.0044; found 324.0014.

N-(2-(Trifluoromethyl)phenyl)-2-(quinolin-2-ylmethylene)hydrazinecarbothioamide (TSC17). TSC17 was prepared from **B17** according to general procedure (method A). Yield: 67%. ^{1}H NMR (300 MHz, DMSO-d_6): δ 12.37 (s, 1H), 10.30 (s, 1H), 8.50 (d, $J = 6.6$ Hz, 1H), 8.38 (d, $J = 6.6$ Hz, 1H), 8.32 (s, 1H), 8.03−7.96 (m, 2H), 7.80−7.72 (m, 3H), 7.63−7.55 (m, 3H). MS (EI, *m/z*): 374 [M]$^+$. HRMS (EI): calcd for C$_{18}$H$_{13}$F$_3$N$_4$S [M]$^+$, 374.0813; found 374.0806.

N-(4-(Trifluoromethyl)phenyl)-2-(quinolin-2-ylmethylene)hydrazinecarbothioamide (TSC18). TSC18 was prepared from **B18** according to general procedure (method A). Yield: 54%. ^{1}H NMR (300 MHz, DMSO-d_6): δ 12.40 (s, 1H), 10.55 (s, 1H), 8.59 (d, $J = 6.6$ Hz, 1H), 8.41 (d, $J = 6.6$ Hz, 1H), 8.34 (s, 1H), 8.03−7.96 (m, 2H), 7.87 (d, $J = 6.3$ Hz, 2H), 7.78−7.72 (m, 3H), 7.65−7.63 (m, 1H). MS (EI, *m/z*): 374 [M]$^+$. HRMS (EI): calcd for C$_{18}$H$_{13}$F$_3$N$_4$S [M]$^+$, 374.0813; found 374.0819.

N-(4-Cyanophenyl)-2-(quinolin-2-ylmethylene)hydrazinecarbothioamide (TSC19). TSC19 was prepared from **B19** according to general procedure (method A). Yield: 49%. ^{1}H NMR (300 MHz, DMSO-d_6): δ 12.46 (s, 1H), 10.56 (s, 1H), 8.57 (d, $J = 6.9$ Hz, 1H), 8.41 (d, $J = 6.9$ Hz, 1H), 8.35 (s, 1H), 8.03−7.98 (m, 2H), 7.89 (dd, $J = 18$ Hz, 6.6 Hz, 4H), 7.79−7.75 (m, 1H), 7.62 (t, $J = 6.0$ Hz, 1H). MS (EI, *m/z*): 331 [M]$^+$. HRMS (EI): calcd for C$_{18}$H$_{13}$N$_5$S [M]$^+$, 331.0892; found 331.0885.

N-(2,6-Diisopropylphenyl)-2-(quinolin-2-ylmethylene)hydrazinecarbothioamide (TSC20). TSC20 was prepared from **B20** according to general procedure (method A). Yield: 57%. ^{1}H NMR (300 MHz, DMSO-d_6): δ 12.13 (s, 1H), 10.10 (s, 1H), 8.65 (d, $J = 9.0$ Hz, 1H), 8.38 (d, $J = 8.7$ Hz, 1H), 8.33 (s, 1H), 8.06−7.61 (m, 4H), 7.36−7.18 (m, 3H), 3.11−3.04 (m, 2H), 1.24−1.15 (m, 12H). MS (EI, *m/z*): 390 [M]$^+$. HRMS (EI): calcd for C$_{23}$H$_{26}$N$_4$S [M]$^+$, 390.1878; found 390.1882.

N-(2-Methoxy-5-methylphenyl)-2-(quinolin-2-ylmethylene)hydrazinecarbothioamide (TSC21). TSC21 was prepared from **B21** according to general procedure (method A). Yield: 40%. ^{1}H NMR (300 MHz, DMSO-d_6): δ 12.22 (s, 1H), 10.10 (s, 1H), 8.40−8.39 (m, 2H), 8.30 (s, 1H), 8.03−7.97 (m, 2H), 7.78−7.62 (m, 3H), 7.03−6.98 (m, 2H), 3.82 (s, 3H), 2.25 (s, 3H). MS (EI, *m/z*): 350 [M]$^+$. HRMS (EI): calcd for C$_{19}$H$_{18}$N$_4$OS [M]$^+$, 350.1201; found 350.1202.

N-Benzyl-2-(quinolin-2-ylmethylene)hydrazinecarbothioamide (TSC22). TSC22 was prepared from **B22** according to general procedure (method A). Yield: 50%. ^{1}H NMR (300 MHz, DMSO-d_6): δ 12.01 (s, 1H), 9.42 (s, 1H), 8.49 (d, $J = 6.0$ Hz, 1H), 8.39 (d, $J = 6.0$ Hz, 1H), 8.28 (s, 1H), 8.01 (t, $J = 9.0$ Hz, 2H), 7.81−7.76 (m, 1H), 7.65−7.61 (m, 1H), 7.41−7.26 (m, 5H), 4.91−4.89 (d, $J = 6.0$ Hz, 2H). MS (EI, *m/z*): 324 [M]$^+$. HRMS (EI): calcd for C$_{18}$H$_{16}$N$_4$S [M]$^+$, 320.1096; found 324.1095.

2-(Quinolin-2-ylmethylene)hydrazinecarbothioamide (TSC24). TSC24 was prepared according to general procedure (method B). Yield: 83%. ^{1}H NMR (400 Hz, DMSO-d_6) δ: 8.37 (2H, $J = 9.6$ Hz, q), 8.20 (1H, s), 7.97 (2H, $J = 8.1$ Hz, t), 7.75 (1H, $J = 8.1$ Hz, t), 7.59 (1H, $J = 8.1$ Hz, t). MS (EI, *m/z*): 230 [M]$^+$. HRMS (EI): calcd for C$_{11}$H$_{10}$N$_4$S [M]$^+$, 230.0626; found, 230.0630.

N,N-Dimethyl-2-(quinolin-2-ylmethylene)hydrazinecarbothioamide (TSC24). TSC24 was prepared according to general procedure (method B). Yield: 92%. ^{1}H NMR (400 Hz, CCl$_3$D) δ: 8.34 (1H, $J = 8.5$ Hz, d), 7.90 (2H, $J = 8.0$ Hz, t), 7.79 (1H, m), 7.70 (1H, s), 7.65 (1H, m), 7.56 (2H, $J = 7.5$ Hz, d), 3.62 (6H, s). MS (EI, *m/z*): 258 [M]$^+$. HRMS (EI): calcd for C$_{13}$H$_{14}$N$_4$S [M]$^+$, 258.0939; found, 258.0934.

2-(Quinoxalin-2-ylmethylene)hydrazinecarbothioamide (TSC25). TSC25 was prepared according to general procedure (method B). Yield: 90%. ^{1}H NMR (400 Hz, DMSO-d_6) δ: 9.79 (1H, s),

8.20 (1H, s), 7.97 (2H, m), 7.81 (2H, m). MS (EI, *m/z*): 231 [M]$^+$. HRMS (EI): calcd for C$_{10}$H$_9$N$_5$S [M]$^+$, 231.0579; found, 231.0578.

N,N-Dimethyl-2-(quinoxalin-2-ylmethylene)hydrazinecarbothioamide (TSC26). TSC26 was prepared according to general procedure (method B). Yield: 93%. ^{1}H NMR (400 Hz, CCl$_3$D) δ: 9.01 (1H, s), 7.92 (1H, m), 7.87 (2H, m), 7.82 (1H, s), 7.18 (1H, m), 3.61 (6H, s). MS (EI, *m/z*): 259 [M]$^+$. HRMS (EI): calcd for C$_{12}$H$_{13}$N$_5$S [M]$^+$, 259.0892; found, 259.0884.

2-((1,8-Naphthyridin-2-yl)methylene)hydrazinecarbothioamide (TSC27). TSC27 was prepared according to general procedure (method B). Yield: 80%. ^{1}H NMR (400 Hz, DMSO-d_6) δ: 9.08 (1H, $J = 4.4$ Hz, 2.0 Hz, dd), 8.48 (3H, m), 8.26 (1H, s), 7.63 (1H, $J = 4.4$ Hz, q). MS (EI, *m/z*): 231 [M]$^+$. HRMS (EI): calcd for C$_{10}$H$_9$N$_5$S [M]$^+$, 231.0579; found, 231.0581.

2-((1,8-Naphthyridin-2-yl)methylene)-N,N-dimethylhydrazinecarbothioamide (TSC28). TSC28 was prepared according to general procedure (method B). Yield: 89%. ^{1}H NMR (400 Hz, DMSO-d_6) δ: 9.08 (1H, $J = 4.4$ Hz, 2.0 Hz, dd), 8.47 (2H, $J = 8.4$ Hz, d), 8.41 (1H, s), 7.62 (1H, $J = 4.4$ Hz, q), 3.35 (6H, s). MS (EI, *m/z*): 259 [M]$^+$. HRMS (EI): calcd for C$_{12}$H$_{13}$N$_5$S [M]$^+$, 259.0892; found, 259.0885.

2-(Benzo[*b*]thiophen-2-ylmethylene)hydrazinecarbothioamide (TSC29). TSC29 was prepared according to general procedure (method B). Yield: 79%. ^{1}H NMR (400 Hz, DMSO-d_6) δ: 8.35 (1H, s), 7.92 (1H, m), 7.83 (1H, m), 7.77 (1H, s), 7.39 (2H, m). MS (EI, *m/z*): 235 [M]$^+$. HRMS (EI): calcd for C$_{10}$H$_9$N$_3$S$_2$ [M]$^+$, 235.0238; found, 235.0234.

2-(Bbenzo[*d*]thiazol-2-ylmethylene)hydrazinecarbothioamide (TSC30). TSC30 was prepared according to general procedure (method B). Yield: 82%. ^{1}H NMR (400 Hz, DMSO-d_6) δ: 8.36 (1H, s), 8.06 (2H, $J = 7.5$ Hz, q), 7.51 (2H, m). MS (EI, *m/z*): 236 [M]$^+$. HRMS (EI): calcd for C$_9$H$_8$N$_4$S$_2$ [M]$^+$, 236.0190; found, 236.0190.

2-(Benzo[*d*]thiazol-2-ylmethylene)-N,N-dimethylhydrazinecarbothioamide (TSC31). TSC31 was prepared according to general procedure (method B). Yield: 87%. ^{1}H NMR (400 Hz, DMSO-d_6) δ: 8.46 (1H, s), 8.06 (2H, $J = 7.5$ Hz, q), 7.50 (2H, m), 3.35 (6H, s). MS (EI, *m/z*): 264 [M]$^+$. HRMS (EI): calcd for C$_{11}$H$_{12}$N$_4$S$_2$ [M]$^+$, 264.0503; found, 264.0506.

2-(Thieno[2,3-*b*]pyridin-2-ylmethylene)hydrazinecarbothioamide (TSC32). TSC32 was prepared according to general procedure (method B). Yield: 91%. ^{1}H NMR (400 Hz, DMSO-d_6) δ: 8.54 (1H, $J = 5.0$ Hz, 1.5 Hz, dd), 8.34 (1H, s), 8.22 (1H, $J = 8.0$ Hz, 1.5 Hz, dd), 7.74 (1H, s), 7.41 (1H, $J = 5.0$ Hz, q). MS (EI, *m/z*): 236 [M]$^+$. HRMS (EI): calcd for C$_9$H$_8$N$_4$S$_2$ [M]$^+$, 236.0190; found, 236.0172.

N,N-Dimethyl-2-(thieno[2,3-*b*]pyridin-2-ylmethylene)hydrazinecarbothioamide (TSC33). TSC33 was prepared according to general procedure (method B). Yield: 80%. ^{1}H NMR (400 Hz, DMSO-d_6) δ: 8.57 (1H, $J = 5.0$ Hz, 1.5 Hz, dd), 8.38 (1H, s), 8.24 (1H, $J = 5.0$ Hz, 1.5 Hz, dd), 7.80 (1H, s), 7.42 (1H, $J = 5.0$ Hz, q), 3.22 (6H, s). MS (EI, *m/z*): 264 [M]$^+$. HRMS (EI): calcd for C$_{11}$H$_{12}$N$_4$S$_2$ [M]$^+$, 264.0503; found, 264.0488.

2-((3,4-Dimethylthieno[2,3-*b*]thiophen-2-yl)methylene)hydrazinecarbothioamide (TSC34). TSC34 was prepared according to general procedure (method B). Yield: 78%. ^{1}H NMR (400 Hz, DMSO-d_6) δ: 8.41 (1H, s), 7.16 (1H, s), 2.47 (3H, s), 2.43 (3H, s). MS (EI, *m/z*): 269 [M]$^+$. HRMS (EI): calcd for C$_{10}$H$_{11}$N$_3$S$_3$ [M]$^+$, 269.0115; found, 269.0126.

2-(Benzo[*h*][1,6]naphthyridin-5-ylmethylene)hydrazinecarbothioamide (TSC35). TSC35 was prepared according to general procedure (method B). Yield: 93%. ^{1}H NMR (400 Hz, DMSO-d_6) δ: 10.29 (1H, s), 9.52 (1H, $J = 8.5$ Hz, 1.3 Hz, dd), 9.06 (1H, $J = 8.5$ Hz, d), 8.38 (1H, $J = 7.6$ Hz, d), 8.16 (1H, $J = 8.5$ Hz, d), 7.91 (3H, m). MS (EI, *m/z*): 281 [M]$^+$. HRMS (EI): calcd for C$_{14}$H$_{11}$N$_5$S [M]$^+$, 281.0735; found, 281.0736.

2-(Benzo[*h*][1,6]naphthyridin-5-ylmethylene)-N,N-dimethylhydrazinecarbothioamide (TSC36). TSC36 was prepared according to general procedure (method B). Yield: 88%. ^{1}H NMR

(400 Hz, DMSO-d_6) δ: 10.35 (1H, J = 8.5 Hz, 1.3 Hz, dd), 9.21 (1H, J = 4.3 Hz, 1.3 Hz, dd), 9.06 (1H, d), 8.66 (1H, s), 8.12 (1H, J = 7.6 Hz, d), 7.85 (3H, m), 3.36 (6H, s). MS (EI, m/z): 309 $[M]^+$. HRMS (EI): calcd for $C_{16}H_{15}N_5S$ $[M]^+$, 309.1048; found, 309.1048.

5.2. Pharmacology. Desferrioxamine (DFO), etoposide (VP16), adriamycin (ADR), and camptothecin (CPT) were purchased from Sigma (St. Louis, MO). All the compounds were dissolved in DMSO at 10 mM, and aliquots were stored at −20 °C. The stock solutions were diluted to the desired concentrations immediately before each experiment. Purified human Topo I and Topo II and kinetoplast DNA (kDNA) were obtained from TopoGEN (Port Orange, FL).

5.2.1. Cell Culture. Human gastric adenocarcinoma SGC-7901, hepatocellular carcinoma BEL-7402, and SMMC-7721 were obtained from the cell bank of the Shanghai Institute of Materia Medica, Chinese Academy of Science (Shanghai, China). Colorectal carcinoma HT-29, HCT116, and LoVo, breast carcinoma MDA-MB-231 and MCF-7, lung adenocarcinoma A549 and NCI-H23, leukemia HL-60, HL-60/MX2, and K562, oral epidermoid carcinoma KB, cervical carcinoma HeLa, and melanoma A375 were purchased from American Type Culture Collection (ATCC, Manassas, VA). Human gastric adenocarcinoma MKN-28 and MKN-45, leukemia U937, and breast carcinoma MDB-MB-435 were obtained from the Japanese Foundation of Cancer Research (Tokyo, Japan). Rhabdomyosarcoma Rh30 cell line was a gift from St. Jude Children's Research. Doxorubicin-selected multidrug resistant (MDR) cell sublines K562/A02 and MCF-7/ADR were purchased from the Institute of Hematology, Chinese Academy of Medical Science. The vincristine (VCR)-selected MDR subline KB/VCR was obtained from the Zhongshan University of Medical Sciences (Guangzhou, China). All these cell lines were maintained in RPMI 1640 medium, containing 10% heat-inactivated fetal bovine serum (Gibco, Grand Island, NY), 100 units/mL penicillin, and 100 μg/mL streptomycin in a humidified atmosphere of 5% CO_2 at 37 °C. MCF-7 and MCF-7/ADR cells were incubated in the medium further supplemented with 1 mM sodium pyruvate and 0.01 mg/mL bovine insulin.

Supporting Information Available: Table S1 listing the HPLC reports for the purity check of all the compounds, as measured in two different mobile phases; Figure S1 showing the effect of TSC24 on Topo IIα-mediated ATP hydrolysis. This material is available free of charge via the Internet at http://pubs.acs.org.

References

(1) Easmon, J.; Purstinger, G.; Heinisch, G.; Roth, T.; Fiebig, H. H.; Holzer, W.; Jager, W.; Jenny, M.; Hofmann, J. Synthesis, cytotoxicity, and antitumor activity of copper(II) and iron(II) complexes of (4)N-azabicyclo[3.2.2]nonane thiosemicarbazones derived from acyl diazines. *J. Med. Chem.* **2001**, *44*, 2164–2171.

(2) Klaymann, D. L.; Scovill, J. P.; Bartosevich, J. F.; Mason, C. J. 2-Acetylpyridine thiosemicarbazones. 2. N4,N4-Disubstituted derivatives as potential antimalarial agents. *J. Med. Chem.* **1979**, *22*, 1367–1373.

(3) Shipman, C., Jr.; Smith, S. H.; Drach, J. C.; Klayman, D. L. Thiosemicarbazones of 2-acetylpyridine, 2-acetylquinoline, 1-acetylisoquinoline, and related compounds as inhibitors of herpes simplex virus in vitro and in a cutaneous herpes guinea pig model. *Antiviral Res.* **1986**, *6*, 197–222.

(4) Shipman, C., Jr.; Smith, S. H.; Drach, J. C.; Klayman, D. L. Antiviral activity of 2-acetylpyridine thiosemicarbazones against herpes simplex virus. *Antimicrob. Agents Chemother.* **1981**, *19*, 682–685.

(5) Jutten, P.; Schumann, W.; Hartl, A.; Dahse, H. M.; Grafe, U. Thiosemicarbazones of formyl benzoic acids as novel potent inhibitors of estrone sulfatase. *J. Med. Chem.* **2007**, *50*, 3661–3666.

(6) Yogeeswari, P.; Sriram, D.; Thirumurugan, R.; Raghavendran, J. V.; Sudhan, K.; Pavana, R. K.; Stables, J. Discovery of N-(2,6-dimethylphenyl)-substituted semicarbazones as anticonvulsants: hybrid pharmacophore-based design. *J. Med. Chem.* **2005**, *48*, 6202–6211.

(7) Greenbaum, D. C.; Mackey, Z.; Hansell, E.; Doyle, P.; Gut, J.; Caffrey, C. R.; Lehrman, J.; Rosenthal, P. J.; McKerrow, J. H.; Chibale, K. Synthesis and structure−activity relationships of parasiticidal thiosemicarbazone cysteine protease inhibitors against *Plasmodium falciparum*, *Trypanosoma brucei*, and *Trypanosoma cruzi*. *J. Med. Chem.* **2004**, *47*, 3212–3219.

(8) Agrawal, K. C.; Sartorelli, A. C. The chemistry and biological activity of alpha-(N)-heterocyclic carboxaldehyde thiosemicarbazones. *Prog. Med. Chem.* **1978**, *15*, 321–356.

(9) Brockman, R. W.; Thomson, J. R.; Bell, M. J.; Skipper, H. E. Observations on the antileukemic activity of pyridine-2-carboxaldehyde thiosemicarbazone and thiocarbohydrazone. *Cancer Res.* **1956**, *16*, 167–170.

(10) Ren, S.; Wang, R.; Komatsu, K.; Bonaz-Krause, P.; Zyrianov, Y.; McKenna, C. E.; Csipke, C.; Tokes, Z. A.; Lien, E. J. Synthesis, biological evaluation, and quantitative structure−activity relationship analysis of new Schiff bases of hydroxysemicarbazide as potential antitumor agents. *J. Med. Chem.* **2002**, *45*, 410–419.

(11) Belicchi-Ferrari, M.; Bisceglie, F.; Casoli, C.; Durot, S.; Morgenstern-Badarau, I.; Pelosi, G.; Pilotti, E.; Pinelli, S.; Tarasconi, P. Copper(II) and cobalt(III) pyridoxal thiosemicarbazone complexes with nitroprusside as counterion: syntheses, electronic properties, and antileukemic activity. *J. Med. Chem.* **2005**, *48*, 1671–1675.

(12) Richardson, D. R.; Sharpe, P. C.; Lovejoy, D. B.; Senaratne, D.; Kalinowski, D. S.; Islam, M.; Bernhardt, P. V. Dipyridyl thiosemicarbazone chelators with potent and selective antitumor activity form iron complexes with redox activity. *J. Med. Chem.* **2006**, *49*, 6510–6521.

(13) Ludwig, J. A.; Szakacs, G.; Martin, S. E.; Chu, B. F.; Cardarelli, C.; Sauna, Z. E.; Caplen, N. J.; Fales, H. M.; Ambudkar, S. V.; Weinstein, J. N.; Gottesman, M. M. Selective toxicity of NSC73306 in MDR1-positive cells as a new strategy to circumvent multidrug resistance in cancer. *Cancer Res.* **2006**, *66*, 4808–4815.

(14) Duffy, K. J.; Shaw, A. N.; Delorme, E.; Dillon, S. B.; Erickson-Miller, C.; Giampa, L.; Huang, Y.; Keenan, R. M.; Lamb, P.; Liu, N.; Miller, S. G.; Price, A. T.; Rosen, J.; Smith, H.; Wiggall, K. J.; Zhang, L.; Luengo, J. I. Identification of a pharmacophore for thrombopoietic activity of small, non-peptidyl molecules. 1. Discovery and optimization of salicylaldehyde thiosemicarbazone thrombopoietin mimics. *J. Med. Chem.* **2002**, *45*, 3573–3575.

(15) Kalinowski, D. S.; Yu, Y.; Sharpe, P. C.; Islam, M.; Liao, Y. T.; Lovejoy, D. B.; Kumar, N.; Bernhardt, P. V.; Richardson, D. R. Design, synthesis, and characterization of novel iron chelators: structure−activity relationships of the 2-benzoylpyridine thiosemicarbazone series and their 3-nitrobenzoyl analogues as potent antitumor agents. *J. Med. Chem.* **2007**, *50*, 3716–3729.

(16) Chen, J.; Huang, Y. W.; Liu, G.; Afrasiabi, Z.; Sinn, E.; Padhye, S.; Ma, Y. The cytotoxicity and mechanisms of 1,2-naphthoquinone thiosemicarbazone and its metal derivatives against MCF-7 human breast cancer cells. *Toxicol. Appl. Pharmacol.* **2004**, *197*, 40–48.

(17) Lindsley, J. E. Use of a real-time, coupled assay to measure the ATPase activity of DNA topoisomerase II. *Methods Mol. Biol.* **2001**, *95*, 57–64.

(18) Le, N. T.; Richardson, D. R. The role of iron in cell cycle progression and the proliferation of neoplastic cells. *Biochim. Biophys. Acta* **2002**, *1603*, 31–46.

(19) Richardson, D. R. Potential of iron chelators as effective antiproliferative agents. *Can. J. Physiol. Pharmacol.* **1997**, *75*, 1164–1180.

(20) Whitnall, M.; Howard, J.; Ponka, P.; Richardson, D. R. A class of iron chelators with a wide spectrum of potent antitumor activity that overcomes resistance to chemotherapeutics. *Proc. Natl. Acad. Sci. U.S.A.* **2006**, *103*, 14901–14906.

(21) Richardson, D. R.; Kalinowski, D. S.; Richardson, V.; Sharpe, P. C.; Lovejoy, D. B.; Islam, M.; Bernhardt, P. V. 2-Acetylpyridine thiosemicarbazones are potent iron chelators and antiproliferative agents: redox activity, iron complexation and characterization of their antitumor activity. *J. Med. Chem.* **2009**, *52*, 1459–1470.

(22) Bernhardt, P. V.; Sharpe, P. C.; Islam, M.; Lovejoy, D. B.; Kalinowski, D. S.; Richardson, D. R. Iron chelators of the dipyridylketone thiosemicarbazone class: precomplexation and transmetalation effects on anticancer activity. *J. Med. Chem.* **2009**, *52*, 407–415.

(23) Antholine, W.; Knight, J.; Whelan, H.; Petering, D. H. Studies of the reaction of 2-formylpyridine thiosemicarbazone and its iron and copper complexes with biological systems. *Mol. Pharmacol.* **1977**, *13*, 89–98.

(24) Chaston, T. B.; Lovejoy, D. B.; Watts, R. N.; Richardson, D. R. Examination of the antiproliferative activity of iron chelators: multiple cellular targets and the different mechanism of action of triapine compared with desferrioxamine and the potent pyridoxal isonicotinoyl hydrazone analogue 311. *Clin. Cancer Res.* **2003**, *9*, 402–414.

(25) Mosmann, T. Rapid colorimetric assay for cellular growth and survival: application to proliferation and cytotoxicity assays. *J. Immunol. Methods* **1983**, *65*, 55–63.

(26) Skehan, P.; Storeng, R.; Scudiero, D.; Monks, A.; McMahon, J.; Vistica, D.; Warren, J. T.; Bokesch, H.; Kenney, S.; Boyd, M. R. New colorimetric cytotoxicity assay for anticancer-drug screening. *J. Natl. Cancer Inst.* **1990**, *82*, 1107–1112.

(27) Hermes-Lima, M.; Nagy, E.; Ponka, P.; Schulman, H. M. The iron chelator pyridoxal isonicotinoyl hydrazone (PIH) protects plasmid pUC-18 DNA against *OH-mediated strand breaks. *Free Radical Biol. Med.* **1998**, *25*, 875–880.

(28) Meng, L. H.; Zhang, J. S.; Ding, J. Salvicine, a novel DNA topo-isomerase II inhibitor, exerting its effects by trapping enzyme−DNA cleavage complexes. *Biochem. Pharmacol.* **2001**, *62*, 733–741.

(29) Singh, N. P.; McCoy, M. T.; Tice, R. R.; Schneider, E. L. A simple technique for quantitation of low levels of DNA damage in individual cells. *Exp. Cell Res.* **1988**, *175*, 184–191.

(30) Lu, H. R.; Zhu, H.; Huang, M.; Chen, Y.; Cai, Y. J.; Miao, Z. H.; Zhang, J. S.; Ding, J. Reactive oxygen species elicit apoptosis by concurrently disrupting topoisomerase II and DNA-dependent protein kinase. *Mol. Pharmacol.* **2005**, *68*, 983–994.

(31) Robinson, M. J.; Martin, B. A.; Gootz, T. D.; McGuirk, P. R.; Moynihan, M.; Sutcliffe, J. A.; Osheroff, N. Effects of quinolone derivatives on eukaryotic topoisomerase II. A novel mechanism for enhancement of enzyme-mediated DNA cleavage. *J. Biol. Chem.* **1991**, *266*, 14585–14592.

(32) Perrin, D.; van Hille, B.; Barret, J. M.; Kruczynski, A.; Etievant, C.; Imbert, T.; Hill, B. T. F 11782, a novel epipodophylloid non-intercalating dual catalytic inhibitor of topoisomerases I and II with an original mechanism of action. *Biochem. Pharmacol.* **2000**, *59*, 807–819.

(33) Osheroff, N. Eukaryotic topoisomerase II. Characterization of enzyme turnover. *J. Biol. Chem.* **1986**, *261*, 9944–9950.

(34) Hu, T.; Sage, H.; Hsieh, T. S. ATPase domain of eukaryotic DNA topoisomerase II. Inhibition of ATPase activity by the anti-cancer drug bisdioxopiperazine and ATP/ADP-induced dimerization. *J. Biol. Chem.* **2002**, *277*, 5944–5951.

(35) Hu, C. X.; Zuo, Z. L.; Xiong, B.; Ma, J. G.; Geng, M. Y.; Lin, L. P.; Jiang, H. L.; Ding, J. Salvicine functions as novel topoisomerase II poison by binding to ATP pocket. *Mol. Pharmacol.* **2006**, *70*, 1593–1601.

(36) Miller, M. C., 3rd; Stineman, C. N.; Vance, J. R.; West, D. X.; Hall, I. H. The cytotoxicity of copper(II) complexes of 2-acetyl-pyridyl-4N-substituted thiosemicarbazones. *Anticancer Res.* **1998**, *18*, 4131–4139.

(37) Carpenter, A. J.; Porter, A. C. Construction, characterization, and complementation of a conditional-lethal DNA topoisomerase II-alpha mutant human cell line. *Mol. Biol. Cell* **2004**, *15*, 5700–5711.

(38) Harker, W. G.; Slade, D. L.; Dalton, W. S.; Meltzer, P. S.; Trent, J. M. Multidrug resistance in mitoxantrone-selected HL-60 leuke-mia cells in the absence of P-glycoprotein overexpression. *Cancer Res.* **1989**, *49*, 4542–4549.

(39) Nitiss, J. L.; Nitiss, K. C. Yeast systems for demonstrating the targets of anti-topoisomerase II agents. *Methods Mol. Biol.* **2001**, *95*, 315–327.

(40) Jensen, P. B.; Sorensen, B. S.; Demant, E. J.; Sehested, M.; Jensen, P. S.; Vindelov, L.; Hansen, H. H. Antagonistic effect of aclarubi-cin on the cytotoxicity of etoposide and 4′-(9-acridinylami-no)methanesulfon-*m*-anisidide in human small cell lung cancer cell lines and on topoisomerase II-mediated DNA cleavage. *Cancer Res.* **1990**, *50*, 3311–3316.

(41) Jensen, P. B.; Sehested, M. DNA topoisomerase II rescue by catalytic inhibitors: a new strategy to improve the antitumor selectivity of etoposide. *Biochem. Pharmacol.* **1997**, *54*, 755–759.

(42) Gieseler, F.; Bauer, E.; Nuessler, V.; Clark, M.; Valsamas, S. Molecular effects of topoisomerase II inhibitors in AML cell lines: correlation of apoptosis with topoisomerase II activity but not with DNA damage. *Leukemia* **1999**, *13*, 1859–1863.

(43) Rogakou, E. P.; Pilch, D. R.; Orr, A. H.; Ivanova, V. S.; Bonner, W. M. DNA double-stranded breaks induce histone H2AX phos-phorylation on serine 139. *J. Biol. Chem.* **1998**, *273*, 5858–5868.

(44) Sehested, M.; Jensen, P. B. Mapping of DNA topoisomerase II poisons (etoposide, clerocidin) and catalytic inhibitors (aclaru-bicin, ICRF-187) to four distinct steps in the topoisomerase II catalytic cycle. *Biochem. Pharmacol.* **1996**, *51*, 879–886.

(45) Woynarowski, J. M.; Sigmund, R. D.; Beerman, T. A. DNA minor groove binding agents interfere with topoisomerase II mediated lesions induced by epipodophyllotoxin derivative VM-26 and acridine derivative m-AMSA in nuclei from L1210 cells. *Biochem-istry* **1989**, *28*, 3850–3855.

(46) Storl, K.; Storl, J.; Zimmer, C.; Lown, J. W. Minor-groove binders are inhibitors of the catalytic activity of DNA gyrases. *FEBS Lett.* **1993**, *317*, 157–162.

(47) Duesbery, N. S.; Webb, C. P.; Leppla, S. H.; Gordon, V. M.; Klimpel, K. R.; Copeland, T. D.; Ahn, N. G.; Oskarsson, M. K.; Fukasawa, K.; Paull, K. D.; Vande Woude, G. F. Proteolytic inactivation of MAP-kinase-kinase by anthrax lethal factor. *Science* **1998**, *280*, 734–737.

(48) Rao, V. A.; Klein, S. R.; Agama, K. K.; Toyoda, E.; Adachi, N.; Pommier, Y.; Shacter, E. B. The iron chelator Dp44mT causes DNA damage and selective inhibition of topoisomerase IIalpha in breast cancer cells. *Cancer Res.* **2009**, *69*, 948–957.

(49) Giles, G. I.; Sharma, R. P. Topoisomerase enzymes as therapeu-tic targets for cancer chemotherapy. *Med. Chem.* **2005**, *1*, 383–394.

(50) Sehested, M.; Jensen, P. B.; Sorensen, B. S.; Holm, B.; Friche, E.; Demant, E. J. Antagonistic effect of the cardioprotector (+)-1,2-bis(3,5-dioxopiperazinyl-1-yl)propane (ICRF-187) on DNA breaks and cytotoxicity induced by the topoisomerase II directed drugs daunorubicin and etoposide (VP-16). *Biochem. Pharmacol.* **1993**, *46*, 389–393.

(51) Chen, M.; Beck, W. T. Teniposide-resistant CEM cells, which express mutant DNA topoisomerase II alpha, when treated with non-complex-stabilizing inhibitors of the enzyme, display no cross-resistance and reveal aberrant functions of the mutant enzyme. *Cancer Res.* **1993**, *53*, 5946–5953.

(52) Jensen, P. B.; Sorensen, B. S.; Sehested, M.; Demant, E. J.; Kjeldsen, E.; Friche, E.; Hansen, H. H. Different modes of anthracycline interaction with topoisomerase II. Separate struc-tures critical for DNA-cleavage, and for overcoming topoiso-merase II-related drug resistance. *Biochem. Pharmacol.* **1993**, *45*, 2025–2035.

(53) Fortune, J. M.; Osheroff, N. Merbarone inhibits the catalytic activity of human topoisomerase IIalpha by blocking DNA clea-vage. *J. Biol. Chem.* **1998**, *273*, 17643–17650.

(54) Gormley, N. A.; Orphanides, G.; Meyer, A.; Cullis, P. M.; Max-well, A. The interaction of coumarin antibiotics with fragments of DNA gyrase B protein. *Biochemistry* **1996**, *35*, 5083–5092.

(55) Gilbert, E. J.; Maxwell, A. The 24 kDa N-terminal sub-domain of the DNA gyrase B protein binds coumarin drugs. *Mol. Microbiol.* **1994**, *12*, 365–373.

(56) Classen, S.; Olland, S.; Berger, J. M. Structure of the topoisomerase II ATPase region and its mechanism of inhibition by the chemo-therapeutic agent ICRF-187. *Proc. Natl. Acad. Sci. U.S.A.* **2003**, *100*, 10629–10634.